Statistical Papers (2025) 66:42
https://doi.org/10.1007/s00362-024-01657-8

REGULAR ARTICLE

Nonparametric testing of first-order structure in point processes on linear networks

Ignacio González-Pérez[1] · María Isabel Borrajo[2] · Wenceslao González-Manteiga[2]

Received: 25 January 2024 / Revised: 5 September 2024

Abstract
In this paper we address a two-sample problem in the context of point processes on linear networks. The aim is to determine whether two given point patterns defined over the same linear network and under the assumption of Poissonness, share the same spatial structure. To do so, a Kolmogorov–Smirnov and a Cramér von Mises type test statistics are developed and analysed through an extensive simulation study. We have included different types of networks, balanced and unbalanced sample sizes, and homogeneous and inhomogeneous Poisson point processes. The results show a good level adjustment and high power values, the latter increasing with the sample size and the discrepancy between the two generating intensities. Finally, these methods have also been applied to the analysis of traffic accidents in Rio de Janeiro (Brazil), studying their distribution at different rush hours.

Keywords Point processes · Linear network · Spatial structure · Two sample problem · Traffic accidents

Mathematics Subject Classification 62G10 · 62G20 · 60G55 · 60-02

1 Introduction

Data sets representing the spatial location of a group of observations are encountered in a wide variety of scenarios, such as trees in a forest, earthquakes in a region, or traffic

✉ María Isabel Borrajo
mariaisabel.borrajo@usc.es

Ignacio González-Pérez
igonzalez@ethz.ch

Wenceslao González-Manteiga
wenceslao.gonzalez@usc.es

1 ETH Zurich, Zurich, Switzerland

2 CITMAga. Department of Statistics, Mathematical Analysis and Optimization, Universidade de Santiago de Compostela, Santiago de Compostela, Spain

Published online: 27 January 2025

(a) Spider webs on the mortar lines of a brick wall.

(b) Dendritic spines on a rat neuron.

(c) Criminal events over Chicago street map.

Fig. 1 Examples of point patterns on linear networks extracted from *spatstat* package

accidents in road networks. Analysing the spatial distribution of these point patterns is crucial in many different fields: ecology (Illian et al. 2009; Law et al. 2009); epidemiology (Lawson 2013); seismology (Ogata and Zhuang 2006; Schoenberg 2003); forestry (Stoyan and Penttinen 2000) or geology (Foxall and Baddeley 2002).

When analysing such patterns, it is important to recognize that the relevant questions pertain not to the observed point patterns themselves, but to the underlying stochastic processes, point processes, that generate these patterns.

Spatial point processes have been widely studied over the years with general references including Daley and Vere-Jones (2003), Diggle (2013) and Cressie (2015). In the last decades, the analysis of point processes on network structures has gathered significant attention. Figure 1 illustrates three examples of this type of data extracted from Baddeley et al. (2015). The linear network framework offers a powerful means of understanding phenomena such as traffic accidents or street crimes. Using this geometric framework allows a more nuanced understanding of the distribution and dynamics of this type of data. However, formalizing point processes on linear networks presents unique mathematical and computational challenges that require rigorous methodological considerations.

Nonparametric methods for point processes on linear networks usually rely on the estimation of the first-order intensity function and some summary statistics. See Baddeley et al. (2015) for a general overview on point patterns analysis, including a last chapter about linear networks and Baddeley et al. (2021) as a more recent review exclusively on the analysis of point patterns on networks. The latter includes not only kernel methods and nonparametric modelling of the intensity, but also second-order analysis using the K-function, pair correlation function and parametric modelling. Moradi (2018) provides statistical tools to study spatial and spatio-temporal points processes on linear networks through first and second order summary statistics, and corrected versions of some of those are presented in Cronie et al. (2020). Other second-order properties, such as the second-order intensity function and the pair correlation function, are studied in Eckardt and Mateu (2021) and D'Angelo et al. (2023). Following this development of summary statistics, Eckardt and Moradi (2024) review the existing ones for spatial marked point processes and propose some novel versions of them for marked point processes on linear networks. Also a discussion on this previously mentioned paper, can be found in Cronie et al. (2024).

Regarding intensity estimation on linear networks several kernel-based methods have been proposed. Borruso (2005, 2008) constituted the first *ad-hoc* proposals for kernel density estimation (KDE) on linear networks. Xie and Yan (2008) postulate a novel network KDE approach to estimate the density of spatial point events without taking the topography of the network into consideration. This results into a kernel which is not a probability density on the network and an extremely biased estimator. Okabe et al. (2009) defined the Equal-Split Kernel Density Estimators (continuous and discontinuous). The former has better statistical properties with a slow computational time, while the latter is faster but with not so good properties. Summarised information about these proposals can be consulted in Okabe and Sugihara (2012).

McSwiggan et al. (2017) defined a new KDE on the network based on the heat equation, which has the advantage of speed up its computation by numerically solving the time-dependent heat equation on the network. Also an extension of Diggle's nonparametric edge-corrected kernel-based intensity estimator was proposed in Moradi et al. (2018), where its statistical properties were detailed (bias, variance and also bandwidth selection methods). An extension of Borruso (2008) to estimate a probability density or a point process intensity on a network based on two-dimensional kernels is proposed in Rakshit et al. (2019). In addition to theoretical results such as consistency and slightly suboptimal efficiency, one important advantage is that Fast Fourier Transform (FFT) can be used to reduce its computational cost. This allows to deal with complex network features and higher volume of data.

In addition to kernel methods, other nonparametric alternatives, such as Voronoi estimators, have been developed, see Okabe and Sugihara (2012) for an initial approach, and Moradi et al. (2019) for a resample-smoothing version of Voronoi intensity estimators.

On the real line and in spatial domains, Poisson point processes are often considered the baseline model. Notice that we cannot distinguish between heterogeneity and interaction in an observed point pattern unless we have some additional information, such as a parametric model, see Diggle (2013). Fuentes-Santos et al. (2016) have noted that the common practice in the analysis of spatial point patterns involves initially assuming the point process is Poisson. This is because the Poisson process serves as a convenient and flexible starting point due to its simplicity and well-defined properties. Researchers typically begin by estimating the first-order intensity, as this provides a basic understanding of the process's average rate of occurrence over the study region. Subsequently, second-order properties, such as the pair correlation function or Ripley's K-function, are estimated to test the Poisson assumption. This two-step approach allows for a straightforward initial analysis, with the second step offering a more detailed examination of the spatial dependence structure. Therefore, the Poisson assumption is generally not considered very restrictive in practice, as it provides a useful baseline for further investigation. Hence, our proposals are defined under this assumption, for which our procedures are well defined, and we are able to derive a convenient resampling scheme for their calibration. The extension of the tests to non-Poisson scenarios may also be possible by determining an appropriate method for the calibration. Some comments on this have been included in the discussion, see Sect. 6.

A vastly studied problem in statistics is population comparison, i.e., determine whether two (or more) samples are generated by the same process, which is com-

monly known as two(or k)-sample problem. This is a very interesting problem with many applications such as change-point detection, or in machine learning determining whether or not a new incoming testing batch of data samples follows the same distribution as the training ones.

These problems have been addressed so far from different perspectives: comparison of characteristic functions (Alba-Fernández et al. 2008), density functions (Anderson et al. 1994) and distribution functions (Finner and Gontscharuk 2018).

The two(or k)-sample problem also arises when dealing with point processes. Let us think for example in the distribution of two species of flora in a region of a forest, outbreaks of natural/caused forest fires, or car-car and car-motorcycle collisions in a road network. In the spatial point processes domain, this comparison problem has already been addressed. Zhang and Zhuang (2017) defined a Kolmogorov–Smirnov type statistic; Fuentes-Santos et al. (2023) proposed a test based on quadratic distance and another one based on the relative risk function, and in Borrajo et al. (2020) a statistic is developed for the comparison of intensity functions when spatial covariates are present. Recently, some advances have been made in solving this two-sample problem on manifolds: a nonparametric test statistic using the Delaunay triangularization is proposed in Gu et al. (2024), and an energy test statistic in Chu and Dai (2024).

The already-introduced two-sample problem applies also when studying point processes on linear networks, recall for example the car-car and car-motorcycle collisions. However, as far as we know, testing methods have not yet been developed for this specific context. Here, this so far untreated problem of comparing the spatial structure of point processes on linear networks is addressed. We propose two specific testing methods that allow us to determine whether two Poisson point processes, located on the same linear network, share a proportional first-order intensity function and, therefore, are generated by the same underlying stochastic process.

The paper is organised as follows: Sect. 2 is devoted to define the theoretical framework in which the methodology is developed. In Sect. 3 we present the characteristics of the two-sample problem on linear networks and we detail our proposed test statistics. Section 4 sums up the results of an extensive simulation study analysing the finite-sample behaviour of our proposals, and in Sect. 5 the application to the real data set is performed. Finally, in Sect. 6 our conclusions are presented and we also discuss about the limitations and possible further extensions of the proposed methods.

2 Preliminaries

2.1 Point processes on linear networks

Throughout this manuscript, a linear network $\mathcal{G}$ is defined as the union of a finite number of segments, with their endpoints serving as nodes. Formally, $\mathcal{G} = (\mathcal{N}, \mathcal{E})$ is a pair where $\mathcal{N} = \{\boldsymbol{v}_1, \ldots, \boldsymbol{v}_{n_n}\} \subset \mathbb{R}^2$ are the nodes and $\mathcal{E} = \{l_1, \ldots, l_{n_e}\}$ are the edges. Recall that these edges start and end at nodes and can only intersect at these points:

$$\forall i \in \{1, \ldots, n_e\}\ \exists\, \boldsymbol{v}_{i_1}, \boldsymbol{v}_{i_2} \in \mathcal{N} :\ \boldsymbol{v}_{i_1} \neq \boldsymbol{v}_{i_2} \text{ and } l_i = \{(1-t)\boldsymbol{v}_{i_1} + t\boldsymbol{v}_{i_2} \in \mathbb{R}^2 : t \in [0, 1]\}.$$

A graph theoretic interpretation of every linear network is also possible, see Eckardt and Mateu (2018) for a more detailed description of this alternative approach with an application to crime-related data.

Another possible extension of linear networks involves relaxing the condition that a linear network consists of a finite union of straight-line segments that intersect only at vertices. Allowing these segments to be replaced by parameterized rectifiable curves, which may or may not overlap, grants more flexibility. This concept has been formalised in Anderes et al. (2020). Additionally, some advances on defining nearest-neighbour point processes on graphs with Euclidean edges can be found in van Lieshout (2018), which is based on a previous conference talk by Jesper Møller in 2016. Although some advances on point processes on graphs with Euclidean edges have been made, most statistical methods have (so far) only been developed and implemented for linear networks, hence, in this work we restrict ourselves to the latter.

Let $\mathcal{L}_\mathcal{G} = \bigcup_{i=1}^{n_e} l_i \subset \mathbb{R}^2$ denote the subset of $\mathbb{R}^2$ represented by a network as the union of its edges, which is assumed to be connected. Moreover, given any subset $\mathcal{L}'_\mathcal{G} \subset \mathcal{L}_\mathcal{G}$, $|\mathcal{L}'_\mathcal{G}|$ denotes the total length of $\mathcal{L}'_\mathcal{G}$, which is the sum of the lengths of all segments in $\mathcal{L}'_\mathcal{G}$. The distance between any two points, $\boldsymbol{v}, \boldsymbol{w} \in \mathcal{L}_\mathcal{G}$, is measured by the shortest path distance, which is the minimum length of all the possible paths between $\boldsymbol{v}$ and $\boldsymbol{w}$, and it is denoted by $d_\mathcal{G}(\boldsymbol{v}, \boldsymbol{w})$. The computation of the shortest path between two nodes of a linear network is a linear programming problem. The most widespread algorithm for computing this measure is the Dijkstra's algorithm, see Dantzig and Thapa (1997, 2003) for details on this.

With these preliminary concepts established, we can now formally introduce a point process $\mathbf{P}$ on a linear network $\mathcal{G}$, as a random mechanism generating locations in $\mathcal{L}_\mathcal{G} \subset \mathbb{R}^2$, whose realization is a pattern of points $\{\boldsymbol{p}_1, \ldots, \boldsymbol{p}_N\} \subset \mathcal{L}_\mathcal{G}$. We assume $\mathbf{P}$ to be a finite, simple point process on $\mathcal{G}$, such that the total number of events has finite second-order moment, see (Daley and Vere-Jones 2003, Chapter 5). The intensity function, $\lambda : \mathcal{L}_\mathcal{G} \to [0, \infty)$ is defined in this context similarly to what it has been done for spatial point processes, i.e., a point process $\mathbf{P}$ on a linear network $\mathcal{G}$ is said to have intensity λ if:

$$\mathbb{E}\left[N(\mathbf{P} \cap \mathcal{L}'_\mathcal{G})\right] = \int_{\mathcal{L}'_\mathcal{G}} \lambda(\boldsymbol{p}) d\boldsymbol{p}, \quad \forall \mathcal{L}'_\mathcal{G} \subset \mathcal{L}_\mathcal{G}, \tag{1}$$

where we integrate with respect to the arc length. Here, N is the counting measure, so $N(\mathbf{P} \cap \mathcal{L}'_\mathcal{G})$ represents the observed number of events on any measurable subset $\mathcal{L}'_\mathcal{G} \subset \mathcal{L}_\mathcal{G}$. Recall that as we are working on networks, the meaning of the intensity, $\lambda(\boldsymbol{p})$, is now the expected number of points per unit length in the vicinity of location $\boldsymbol{p}$.

As explained in the introduction, various methodologies have been developed to estimate the intensity function of a point process on a linear network, with kernel-based methods being the most prolific. The main disadvantage of these 'pure kernel based' estimators is their high computational cost, which rapidly increases with the number of nodes. To address this issue, a method based on the relationship between kernel smoothing and diffusion, usually referred to as the heat equation estimator, is proposed in McSwiggan et al. (2017). Given a point pattern $\mathbf{p} = \{\boldsymbol{p}_1, \ldots, \boldsymbol{p}_N\}$ on a linear network, this heat kernel estimator admits a kernel sum representation:

$$\widehat{\lambda}(\boldsymbol{p}) = \sum_{i=1}^{N} \kappa_t(\boldsymbol{p}|\boldsymbol{p}_i),$$

where $\kappa_t(\boldsymbol{p}|\boldsymbol{q})$ is the heat kernel, the probability density at time t^2 of a particle executing a Brownian motion on the network starting at location $\boldsymbol{q}$ at time 0. As shown in McSwiggan (2019), the heat kernel estimator is symmetric and is formally equivalent to the Equal-Split continuous intensity estimator, Okabe and Sugihara (2012), when using a Gaussian kernel. In addition, it preserves mass (meaning it integrates to the observed number of point over the entire linear network), and it is unbiased if and only if the true intensity is constant. As mentioned in Rakshit et al. (2019), these properties position the heat kernel estimator as the "canonical" choice for kernel intensity estimation on a linear networks. The diffusion estimator is also considerably more computationally efficient than the Equal-Split continuous estimator, with bandwidth selection methods defined in McSwiggan et al. (2017) and Rakshit et al. (2019).

2.2 Poisson point processes

Poisson point processes have played a crucial role in the development of spatial point process theory. They serve as a fundamental starting point and reference for addressing various problems. As stated in Baddeley et al. (2015), a Poisson point process on a linear network is defined similarly to a Poisson point process in two dimensions. Two types of Poisson point processes can be distinguished: homogeneous and inhomogeneous.

Given a linear network $\mathcal{G} = (\mathcal{N}, \mathcal{E})$ and $\mathcal{L}_\mathcal{G}$ its corresponding subset of $\mathbb{R}^2$, the homogeneous Poisson point process with intensity $\lambda > 0$ verifies that the number of points falling in any subregion, $\mathcal{L}'_\mathcal{G} \subset \mathcal{L}_\mathcal{G}$, follows a Poisson distribution. The expected number of points falling in $\mathcal{L}'_\mathcal{G}$ is $\lambda|\mathcal{L}'_\mathcal{G}|$. Furthermore, given two disjoint subsets $\mathcal{L}'_\mathcal{G}$ and $\mathcal{L}''_\mathcal{G}$ of $\mathcal{L}_\mathcal{G}$, the variables counting the number of events in each subset are independent.

The inhomogeneous Poisson point process extends the homogeneous case by allowing the intensity to vary with location. Thus, the assumptions remain largely the same as in the homogeneous case, with the expected number of points falling in $\mathcal{L}'_\mathcal{G}$ given by (1). For more details about Poisson point processes on linear networks, see (Baddeley et al. 2015, Chapter 17).

3 The proposed methods

Let $\mathbf{P}_1$ and $\mathbf{P}_2$ be two point processes on a linear network $\mathcal{G}$ with counting measures N_i and first-order intensity functions λ_i for $i = 1, 2$. The primary objective of our approach is to determine whether these two point processes share the same underlying spatial structure, specifically whether their intensity functions are proportional. By focusing on proportionality rather than equality, we allow for differences in the overall scale of the intensity functions, meaning the processes can have different mean numbers of points. Proportionality implies that the spatial structure is preserved, with

areas of high and low intensity occurring at corresponding locations across both processes. This approach is particularly useful when absolute intensity levels vary, but the spatial distribution pattern remains consistent.

The main difference between an intensity function and a density function is that the former does not need to be normalized to integrate to one. Given an intensity function $\lambda : \mathcal{L}_{\mathcal{G}} \to \mathbb{R}^+$ for a point process on a linear network $\mathcal{G}$, its relative density is defined as:

$$f_\lambda(\boldsymbol{p}) = \frac{\lambda(\boldsymbol{p})}{\int_{\mathcal{L}_{\mathcal{G}}} \lambda(\boldsymbol{q}) d\boldsymbol{q}}, \quad \forall \boldsymbol{p} \in \mathcal{L}_{\mathcal{G}}.$$

Thus, the problem reduces to comparing these relative density functions. Formally, our testing problem can be written as:

$$\mathcal{H}_0 : \exists\, \eta > 0 \text{ such that } \lambda_1(\boldsymbol{p}) = \eta \lambda_2(\boldsymbol{p})\ \forall \boldsymbol{p} \in \mathcal{L}_{\mathcal{G}} \Leftrightarrow f_{\lambda_1}(\boldsymbol{p}) = f_{\lambda_2}(\boldsymbol{p})\ \forall \boldsymbol{p} \in \mathcal{L}_{\mathcal{G}}. \tag{2}$$

We say that the intensities are proportional with η as the proportional parameter, when (2) holds. The alternative hypothesis is that there exists at least one set of locations with non-zero length on the point processes domain where the intensities of the two processes are not proportional.

Remark 1.- In general, for point processes, the null hypothesis should be formulated in terms of the conditional intensity function, $\lambda_c(\boldsymbol{p}|\boldsymbol{q})$, which represents the intensity of the point process at $\boldsymbol{p} \in \mathcal{L}_{\mathcal{G}}$ conditional on observing a point at $\boldsymbol{q} \in \mathcal{L}_{\mathcal{G}}$, see Diggle (2013). Under a Poisson assumption, both functions are equivalent. Other definitions of the conditional intensity can be found in Baddeley et al. (2015), where the authors consider conditioning on the whole observed pattern. However, the implications for our proposals remain unchanged.

Remark 2.- An important fact in the definition of this testing procedure is that it is based on a Poisson assumption. Hence, testing this condition is essential to obtain an accurate interpretation of the result of the test, i.e., when rejecting the null hypothesis, it is crucial to determine whether the rejection is due to the failure of the Poisson assumption or the falseness of H_0 itself. In practice, tools similar to those available in the R-package *spatstat* to perform the test described in Loosmore and Ford (2006) (`dclf.test`) and Ripley (1977, 2005) (`mad.test`) for the K and L functions should be applied. Although there is not so many specific tools for linear networks, in our real data application we perform some Monte Carlo simulations to build a global envelope for the K-function, see Sect. 5 for more details.

3.1 Kolmogorov–Smirnov type test statistic

This first method is an adaptation of the techniques developed in Zhang and Zhuang (2017) for spatial point processes to linear networks. The idea is to translate the point-to-point proportionality relationship of the null hypothesis in (2) into a relationship between the different possible subsets of the graph, $\mathcal{L}_{\mathcal{G}}$.

An equivalent interpretation of the null hypothesis in (2) using path integration may be written as:

$$\mathbb{E}[N(\mathbf{P}_1 \cap \mathcal{L}'_{\mathcal{G}})] = \int_{\mathcal{L}'_{\mathcal{G}}} \lambda_1(\boldsymbol{p}) d\boldsymbol{p} \overset{\mathcal{H}_0}{=} \eta \int_{\mathcal{L}'_{\mathcal{G}}} \lambda_2(\boldsymbol{p}) d\boldsymbol{p} = \eta \mathbb{E}[N(\mathbf{P}_2 \cap \mathcal{L}'_{\mathcal{G}})], \quad \forall \mathcal{L}'_{\mathcal{G}} \subset \mathcal{L}_{\mathcal{G}}, \tag{3}$$

yielding an estimate of η as $\widehat{\eta} = N_1/N_2$.

Following the ideas in Zhang and Zhuang (2017), an appropriate discrepancy measure based on subsets is defined as:

$$D(\mathcal{L}'_{\mathcal{G}}) = \left| N_1(\mathcal{L}'_{\mathcal{G}}) - \widehat{\eta} N_2(\mathcal{L}'_{\mathcal{G}}) \right| = N_1 \left| \frac{N_1(\mathcal{L}'_{\mathcal{G}})}{N_1} - \frac{N_2(\mathcal{L}'_{\mathcal{G}})}{N_2} \right|, \quad \forall \mathcal{L}'_{\mathcal{G}} \subset \mathcal{L}_{\mathcal{G}}. \tag{4}$$

Thus, a test statistic can be built as the supreme of all possible discrepancies when $\mathcal{L}'_{\mathcal{G}} \subset \mathcal{L}_{\mathcal{G}}$. Exploring the entire Borel σ-algebra of $\mathcal{L}_{\mathcal{G}}$ is too time-consuming. To overcome this, Zhang and Zhuang (2017) proved that taking the supreme of the discrepancies in a π-systems, $\mathcal{S}$, (a non-empty family of subsets closed under intersection of the observation region generating the σ-algebra) is sufficient. Therefore, our test statistic should be of the form

$$\frac{1}{\xi} \sup_{\mathcal{L}'_{\mathcal{G}} \in \mathcal{S}} D(\mathcal{L}'_{\mathcal{G}}),$$

where ξ is an appropriate scaling term to ensure that the test statistic has a standard asymptotic distribution. For spatial point processes the expression of ξ was theoretically derived in Zhang and Zhuang (2017). An analogous result for point processes on linear networks has not yet been developed, so we opt to consider a straightforward adaptation of the estimator of ξ:

$$\widehat{\xi} = \left(\frac{1}{\Gamma - 1} \frac{N_1 + N_2}{N_1 N_2} \sum_{\gamma=1}^{\Gamma} \left[\frac{[N_1(\mathcal{L}_\gamma) - \widehat{N_1}(\mathcal{L}_\gamma)]^2}{\widehat{N_1}(\mathcal{L}_\gamma)} + \frac{[N_2(\mathcal{L}_\gamma) - \widehat{N_2}(\mathcal{L}_\gamma)]^2}{\widehat{N_2}(\mathcal{L}_\gamma)} \right] \right)^{1/2}, \tag{5}$$

where $\{\mathcal{L}_\gamma\}_{\gamma=1}^{\Gamma}$ is a partition of $\mathcal{L}_{\mathcal{G}}$ such that there is at least one point from one of the two observed patterns in every element, and $\widehat{N_i}(\mathcal{L}_\gamma) = N_i \cdot \frac{N_1(\mathcal{L}_\gamma) + N_2(\mathcal{L}_\gamma)}{N_1 + N_2}$. Note that (5) is a discrepancy measure between the number of observed points in every element of the partition using each pattern independently, and the number of observed points combining the two patterns. It is well defined since $\widehat{N_i}(\mathcal{L}_\gamma) > 0$ for $i = 1, 2$ and $\gamma \in \{1, \ldots, \Gamma\}$, because there is at least one observed point in every element of the partition.

The final form of our test statistic is:

$$T_{KS} = \frac{1}{\widehat{\xi}} \sup_{\mathcal{L}'_{\mathcal{G}} \in \mathcal{S}} \left| \frac{N_1(\mathcal{L}'_{\mathcal{G}})}{N_1} - \frac{N_2(\mathcal{L}'_{\mathcal{G}})}{N_2} \right|. \tag{6}$$

When computing (6), both the π-system and the partition of the network must be determined. A natural partition of the network is the set of all edges. However, this

could not be a valid since the existence of events in every edge is not guaranteed. We can overcome this by joining each of the edges with no points to an edge on which a point is observed. This is equivalent to restrict the sum given in Eq. (5) to those edges where at least a point is observed.

The choice of the π-system, $\mathcal{S}$, is not such a straightforward matter. As stated in Zhang and Zhuang (2017), a few options may be obtained using different choices of the π-system, but they are all close to the significance level and the differences are shown in their power values. Relying on this, our proposal here aims to simplify the computation of the proposed Kolmogorov–Smirnov type test statistic on linear networks. Hence, let $\mathcal{S}$ be the set of balls with the shortest path distance in $\mathcal{L}_{\mathcal{G}}$, centred at a point $\boldsymbol{q} \in \mathcal{L}_{\mathcal{G}}$:

$$\mathcal{S} = \{B_{\mathcal{L}_{\mathcal{G}}}(\boldsymbol{q}, r) : r > 0\}, \quad \text{where} \quad B_{\mathcal{L}_{\mathcal{G}}}(\boldsymbol{q}, r) = \{\boldsymbol{p} \in \mathcal{L}_{\mathcal{G}} : d_{\mathcal{G}}(\boldsymbol{p}, \boldsymbol{q}) < r\}. \tag{7}$$

The choice of $\boldsymbol{q}$ should be determined based on the type of linear network in which the events are observed. For connected networks, classification depends on whether the network contains loops or closed paths (paths that start and end at the same node). In networks with loops, a reasonable choice for $\boldsymbol{q}$ is the "centre" of the network, specifically the point on the network closest to the centre of its convex hull. Conversely, for trees (loop-free linear networks that have a distinct base or root node), it is suggested to select $\boldsymbol{q}$ as the root node.

Additionally, the set of radii of these balls needs to be determined. From a theoretical perspective, all positive values $r > 0$ are possible, and thus a supremum is used in the definition of the test statistic, see (6). In practice, these radii can be chosen as the distances from $\boldsymbol{q}$ to all the points in the two observed patterns, and the supremum becomes a maximum.

3.2 Cramér von Mises type test statistic

This second proposal is based on the fact that the null hypothesis in (2) can be framed in terms of the relative densities. Under the null hypothesis, the distance (in a given function space) between these density functions should be zero. Consequently, the quadratic distance between the estimates of the relative density functions can serve as a measure of discrepancy. Specifically if $\widehat{\lambda}_i(\boldsymbol{p})$ represents an estimate of the intensity function of $\mathbf{P}_i$, with $i = 1, 2$, then $\widehat{\lambda}_i(\boldsymbol{p})/N_i$ is an estimate of its relative density function. Our proposed test statistic is therefore given by:

$$T_{CvM} = \int_{\mathcal{L}_{\mathcal{G}}} \left(\frac{\widehat{\lambda}_1(\boldsymbol{p})}{N_1} - \frac{\widehat{\lambda}_2(\boldsymbol{p})}{N_2} \right)^2 d\boldsymbol{p}, \tag{8}$$

where higher values of this statistic indicate greater discrepancy from the null hypothesis.

To compute the statistic in (8), the intensity estimators should ideally be constructed using the same technique to ensure that observed discrepancies are attributable to differences between the point processes rather than to the estimation methods. Moreover,

implementing mass-conserving estimators is crucial for maintaining the accuracy and reliability of point process intensity estimates by preserving the expected number of events across the network.

Once the estimation method is selected, no additional parameters need to be specified for this test statistic, which is an advantage over the previously proposed Kolmogorov–Smirnov type test statistic that requires more parameter selection. However, this approach incurs a higher computational cost. To address this, we use the classical heat kernel method described by McSwiggan et al. (2017), which is analogous to the Gaussian kernel for linear networks and preserves mass. The authors proved that this method, which can be efficiently computed by solving the classical time-dependent heat equation on the network, is equivalent, in certain contexts, to the equal-split continuous estimator. This equivalency offers desirable statistical properties, such as mass conservation and unbiasedness.

As noted by Rakshit et al. (2019), the heat kernel estimator is considered the "canonical" choice for kernel intensity estimation on linear networks. Its performance is slightly superior to the method proposed in Rakshit et al. (2019), which the authors claim that has a suboptimal statistical performance and an inherent limit on spatial resolution. Nevertheless, other intensity estimators discussed in the literature could be applied to the Cramér von Mises type test statistic. In particular, for faster computation on very large networks, the convolution estimator should be considered, despite its slightly suboptimal performance, as detailed in Rakshit et al. (2019).

It is also important to note that the heat kernel estimator relies on a bandwidth parameter, which is selected using the modified Scott's rule. Both, McSwiggan (2019) and Rakshit et al. (2019) assert that simple rules of thumb, such as Scott's, perform reasonably well and are less prone to breakdown. An intriguing open problem is to develop *ad-hoc* bandwidth selectors for this specific testing problem, including comparisons with the modified Scott's rule, cross-validation methods and also a common bandwidth, as used in Davies et al. (2018) for estimating the relative risk function.

3.3 Calibration and computational aspects

The theoretical results establishing the asymptotic distribution of the two test statistics are not yet available. Therefore, permutation methods are employed to calibrate our two proposals. Even when the asymptotic distribution of a test statistic is known, convergence rates are often too slow to be practically useful. For further details on this see González-Manteiga and Crujeiras (2013), where the authors proved that applying asymptotic theory for calibration can presents several challenges: estimating nuisance functions, slow convergence rates, and difficulties in determining the limit distribution. In such cases, permutation methods or bootstrapping techniques offer solutions to these calibration issues.

Permutation testing has been successfully applied in various scenarios within spatial statistics. For example, Corral-Rivas et al. (2010) uses permutations to differentiate between regular, random, and cluster processes; Fuentes-Santos et al. (2018) to test separability in spatio-temporal point processes or Fuentes-Santos et al. (2023)

to address the two-sample problem for spatial point processes. Theoretical results regarding permutation tests are discussed in Pesarin and Salmaso (2010, 2013).

Permutation tests require minimal assumptions and provide an effective means of determining statistical significance without imposing stringent requirements on the generating process. To estimate the sampling distribution of our tests, a large number of samples generated under the null hypothesis is required, where the two underlying processes have proportional intensities. This null hypothesis implies that altering the group assignment of an event has no effect on the outcome. The approach involves repeatedly shuffling the original patterns, randomly assigning group labels (1 or 2), and determining the distribution of the test statistic under the null hypothesis. This process enables us to rank the original test statistic value and compute the corresponding p-value. We outline the following algorithm.

Algorithm 1 Calibration procedure

1: With the original two point patterns of sizes N_1 and N_2, respectively, compute the test statistic using either (6) or (8).
2: Pool together the two original point patterns.
3: Choose N_1 points independently and without repetition, and assign them to pattern number 1. The remaining N_2 points are assigned to pattern number 2.
4: Compute the corresponding test statistic with the new patterns using again the same test statistic, either (6) or (8). This resulting value is a realization from the test statistic's distribution under the null hypothesis.
5: Repeat steps 2 to 4 n_p times leading to a large sample of our test statistic under the null hypothesis. Approximate the critical value of the test at level α by the $[(1-\alpha)n_p]$-th order statistic of those n_p values. Compute the p-value as the proportion of permuted test statistics which are larger than the initially observed one.

In practice, computing the total number of permutations is often infeasible for common sample sizes. Standard practice involves considering a subset of n_p permutations, selected at random from all possible permutations. Selecting an appropriate value for n_p is crucial, as it must be sufficiently large to ensure reliable results while remaining computationally feasible. As discussed in Marozzi (2004), an n_p value of 5000 is generally sufficient, although in some cases, n_p may be increased to $n_p = 10000$. To balance reliable results with computational cost, we have set $n_p = 7500$, which, as shown in Sect. 4, has proved sufficient for our test statistics. It is important to note that the computational cost of permutations increases significantly with the number of nodes in the linear network.

4 Simulation study

In this section, we present a simulation study to evaluate the finite sample performance of our new proposals. Note that no comparisons with potential competitors are made, as this testing problem has not yet been addressed in the specific context of linear networks.

We analyse the level and power of the tests by generating $M = 1000$ Monte Carlo realizations for each scenario.The scenarios include both homogeneous and inhomogeneous Poisson point processes on various linear networks, with expected sample

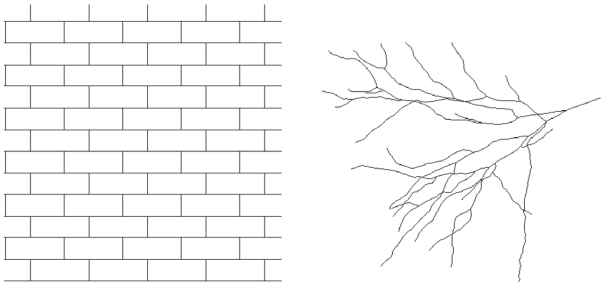

(a) *Spiders*. (b) *Dendrite*.

Fig. 2 Representation of the linear networks, *Spiders* and *Dendrite*, included in the simulation study

sizes ranging from 20 to 750 events. Additionally, both balanced and unbalanced scenarios are considered, where balanced scenarios have the same expected number of points in each pattern, while unbalanced scenarios do not.

First, the network structure must be determined. Two different network structures are considered: one with loops, see Fig. 2a, and one that is a tree, see Fig. 2b. The former, known as *Spiders* and presented in Voss (1999, 2007), while the latter is detailed in Jammalamadaka et al. (2013) and Baddeley et al. (2014), and it is known as *Dendrite*. Both data sets are available in Baddeley and Turner (2005).

Including both networks with and without loops aims to show the effect of the choice of the π-system on the performance of the Kolmogorov–Smirnov type test statistic.

4.1 Models under the null hypothesis

To determine the level adjustment of our proposals, we define Poisson point processes with proportional intensity functions, considering both homogeneous and inhomogeneous scenarios.

Let m denote the expected number of events. The intensity of the homogeneous Poisson point processes is given by:

$$\lambda_{Hom}(\boldsymbol{p}) = \frac{m}{|\mathcal{L}_{\mathcal{G}}|}, \quad \forall \boldsymbol{p} \in \mathcal{L}_{\mathcal{G}}, \tag{9}$$

where $|\mathcal{L}_{\mathcal{G}}|$ denotes the total length of the network.

Additionally, the intensity function for the inhomogeneouos Poisson point process is given by:

$$\lambda_{Inh}(\boldsymbol{p}) = m \cdot \frac{1 - \sqrt[10]{p_2/1125}}{\int_{\mathcal{L}_{\mathcal{G}}} \left(1 - \sqrt[10]{q_2/1125}\right) d\boldsymbol{q}}, \quad \forall \boldsymbol{p} = (p_1, p_2) \in \mathcal{L}_{\mathcal{G}}, \tag{10}$$

which decreases smoothly as the coordinate p_2 increases, see Fig. 3. Note that the denominator represents a path integral where $\boldsymbol{q} = (q_1, q_2) \in \mathcal{L}_{\mathcal{G}}$. Homogeneous

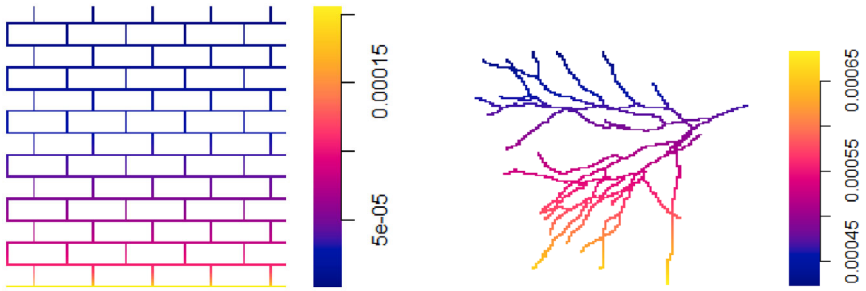

(a) *Spiders*. (b) *Dendrite*.

Fig. 3 Relative density function associated with the inhomogeneous model, λ_{Inh} in (10), over both network structures

models are constant across the network, so their representation is omitted as it does not contribute additional understanding.

To analyse the level adjustment, for each Monte Carlo realization, two point patterns are generated from the same Poisson point process, and the test is performed using permutations. The results from the 1000 Monte Carlo realizations in the balanced scenarios are summarised in Tables 1, 2, 5 and 6 in Sect. 4.3. Similar summaries for the unbalanced scenarios are provided in Appendix A.

4.2 Models under the alternative hypothesis

Once the level is adjusted, to analyse the power of our proposals, Poisson point processes with non-proportional intensity functions are considered. In each scenario, homogeneous and inhomogeneous, the baseline model is the one previously used for the level adjustment, given in (9) and (10), which is denoted by λ_1. We need to define a non-proportional intensity, and to have some degree of control over the discrepancy with respect to the null hypothesis, we build λ_2 from λ_1 by adding a expected events homogeneously distributed in a subregion of $\mathcal{L}_\mathcal{G}$:

$$\lambda_2(\boldsymbol{p}) = \lambda_1(\boldsymbol{p}) + \frac{a}{|\mathcal{L}_\mathcal{G}^+|}\mathbf{1}_{\mathcal{L}_\mathcal{G}^+}(\boldsymbol{p}), \quad \forall \boldsymbol{p} \in \mathcal{L}_\mathcal{G}. \tag{11}$$

We must specify the subregions $\mathcal{L}_\mathcal{G}^+$ of the networks in which those a events are added. The network length in these subregions is chosen to be approximately the same (about 15%) for both linear networks *Spiders* and *Dendrite*. The subregions are defined as follows:

$$\mathcal{L}^+_{Spiders} = \left\{\boldsymbol{p} = (p_1, p_2) \in \mathcal{L}_{Spiders} \colon \boldsymbol{p} \in [337.5,\ 787.5] \times [337.5,\ 787.5]\right\}, \tag{12}$$

and

$$\mathcal{L}^+_{Dendrite} = \{\boldsymbol{p} = (p_1, p_2) \in \mathcal{L}_{Dendrite} \colon \boldsymbol{p} \in [73.02,\ 139.955] \times [242.2,\ 298.3]\}, \tag{13}$$

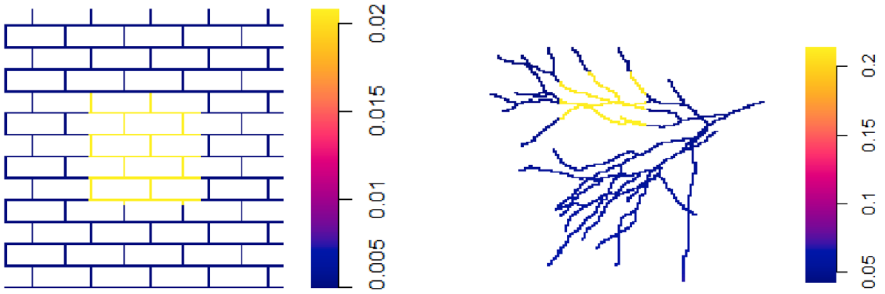

(a) *Spiders*. (b) *Dendrite*.

Fig. 4 For $m = 100$ and $a = 50$, representation of the perturbed homogeneous intensity function according to (11) in both networks

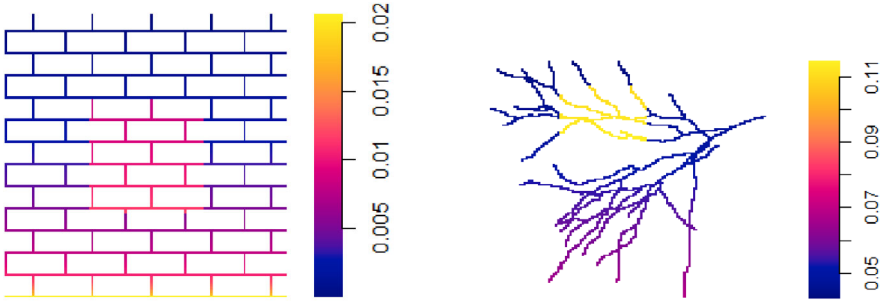

(a) *Spiders*. (b) *Dendrite*.

Fig. 5 For $m = 100$ and $a = 20$, representation of the perturbed inhomogeneous intensity function according to (11) in both networks

where the coordinates are those of the Euclidean plane in which the network is embedded. In Figs. 4 and 5, those λ_2 intensity functions for the homogeneous and inhomogeneous scenarios are represented, where the subregions $\mathcal{L}_\bullet^+$ show the highest intensity values due to the events we have added.

The value of parameter a determines the "distance" from every alternative to the null hypothesis of proportional intensities ($a = 0$). For each of these possible values, the departure from the null hypothesis should be "at the same pace" and thus a depends on m. In our study, a is chosen to be multiples of $m/4$, which allows us to cover a wide range of possible alternative hypothesis.

To study the power values, for each Monte Carlo realisation, one pattern is generated from a Poisson point process with intensity given by the baseline functions λ_1 in (9) and (10) (for the homogeneous and inhomogeneous cases, respectively). A second pattern is generated from a Poisson point process with intensity given by (11), where a is assigned different values to control the discrepancy to the null hypothesis. The results over the 1000 Monte Carlo realizations in the balanced scenarios are summarised in Tables 3, 4, 7 and 8 in Sect. 4.3. Similar summaries for the unbalanced scenarios are included in Appendix A.

4.3 Results

In this section, we summarise the results of the previously introduced simulation study. First, we differentiate between the balanced and unbalanced scenarios. The balanced scenario includes situations in which the expected number of events is the same in the two processes of interest. Conversely, the unbalanced scenario consists of processes with different expected numbers of events. We have included cases with rates of two and four. The results for the unbalanced scenario are provided in A to avoid overloading the main document.

Kolmogorov–Smirnov type statistic

As detailed in Sect. 3.1, a π-system needs to be chosen to compute this test statistic. In (7) we suggest to choose the π-system as a set of concentric balls, where the base point is a crucial aspect. In *Spiders*, we consider the closest point of the network (in Euclidean distance) to the centre of its convex hull, while in *Dendrite* the root node of the tree is chosen. The selection depends, as previously detailed, on the structure of the network (whether it has loops or not). Both are represented in Fig. 6. Furthermore, as suggested in Sect. 3.1, the set of radii are chosen as the distances from $\boldsymbol{q}$ to all the points in the two observed patterns.

Tables 1 and 2 present the calibration performance of the Kolmogorov–Smirnov type test statistic across varying expected sample sizes, m, and nominal significance levels, α, for the two distinct network models: *Spiders* and *Dendrite*. Both homogeneous and inhomogeneous models are considered to evaluate the behaviour of the test statistic under different conditions.

In Tables 1 and 2 the observed rejection proportions closely match the nominal levels for $m \geq 50$, indicating a well-calibrated test. For smaller sample sizes, $m = 20$, there is a slight deviation, especially at $\alpha = 0.01$, where for the inhomogeneous model the observed rejection proportions are slightly lower than the nominal levels, but remain competitive. Thus, the results suggest that the Kolmogorov–Smirnov type test statistic maintains good calibration properties for both network models when the expected sample size is 50 or larger. Even for smaller sample sizes, such as $m = 20$, the test statistic remains competitive, albeit with minor deviations from the nominal levels.

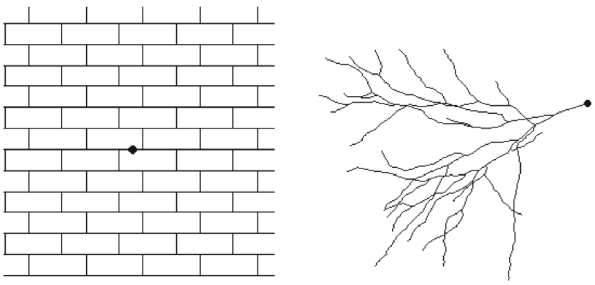

(a) *Spiders*. (b) *Dendrite*.

Fig. 6 Base point (black dot) of the π-system in both network structures

Table 1 Proportion of rejections under the null hypothesis for the Kolmogorov–Smirnov type test statistic on *Spiders*, for both the homogeneous and inhomogeneous models

	Homogeneous model			Inhomogeneous model		
	$\alpha = 0.1$	$\alpha = 0.05$	$\alpha = 0.01$	$\alpha = 0.1$	$\alpha = 0.05$	$\alpha = 0.01$
$m = 20$	0.095	0.049	0.012	0.084	0.037	0.007
$m = 50$	0.093	0.054	0.014	0.099	0.056	0.009
$m = 100$	0.090	0.042	0.009	0.099	0.056	0.009
$m = 200$	0.092	0.040	0.007	0.105	0.050	0.015
$m = 500$	0.107	0.051	0.007	0.107	0.048	0.003

Table 2 Proportion of rejections under the null hypothesis for the Kolmogorov–Smirnov type test statistic on *Dendrite*, for both the homogeneous and inhomogeneous models

	Homogeneous model			Inhomogeneous model		
	$\alpha = 0.1$	$\alpha = 0.05$	$\alpha = 0.01$	$\alpha = 0.1$	$\alpha = 0.05$	$\alpha = 0.01$
$m = 20$	0.112	0.068	0.020	0.093	0.045	0.007
$m = 50$	0.112	0.067	0.015	0.096	0.046	0.010
$m = 100$	0.093	0.058	0.016	0.093	0.050	0.014
$m = 200$	0.094	0.059	0.009	0.097	0.046	0.004
$m = 500$	0.104	0.051	0.015	0.113	0.061	0.012

Table 3 Proportion of rejections for different alternative hypotheses (deviation from the null hypothesis controlled by parameter a) for the Kolmogorov–Smirnov type test statistic on *Spiders*, for both the homogeneous and inhomogeneous models

	Homogeneous model			Inhomogeneous model		
	$a = 3m/4$	$a = m/2$	$a = m/4$	$a = 3m/4$	$a = m/2$	$a = m/4$
$m = 50$	0.915	0.639	0.279	0.972	0.792	0.327
$m = 100$	0.998	0.960	0.536	0.999	0.988	0.618
$m = 200$	1	1	0.856	1	1	0.914
$m = 500$	1	1	0.997	1	1	1

Table 4 Proportion of rejections for different alternative hypotheses (deviation from the null hypothesis controlled by parameter a) for the Kolmogorov–Smirnov type test statistic on *Dendrite*, for both the homogeneous and inhomogeneous models

	Homogeneous model				Inhomogeneous model			
	$a = 7m/4$	$a = 3m/2$	$a = 5m/4$	$a = m$	$a = 7m/4$	$a = 3m/2$	$a = 5m/4$	$a = m$
$m = 50$	0.328	0.319	0.264	0.214	0.350	0.328	0.291	0.245
$m = 100$	0.651	0.616	0.526	0.429	0.675	0.608	0.535	0.445
$m = 200$	0.964	0.937	0.898	0.799	0.963	0.923	0.891	0.813
$m = 500$	1	1	1	1	1	1	1	0.999

These findings indicate the robustness and reliability of the Kolmogorov–Smirnov type test test statistic across different network structures and conditions.

Focusing now on the power of the Kolmogorov–Smirnov type test statistic, Tables 3 and 4 display the empirical power of the Kolmogorov–Smirnov type test statistic under various alternative hypotheses. The power is evaluated across different values of the parameter a, which controls the deviation from the null hypothesis, for two network models: *Spiders* and *Dendrite*. Note that values of parameter a are not the same for the two networks. This is due to the fact that in *Spiders* very high power values are reached for smaller values of a, while in *Dendrite* alternatives that are further away from the null hypothesis are needed. Both homogeneous and inhomogeneous models are again considered.

Table 3 shows that the power of the Kolmogorov–Smirnov type test statistic increases with both the expected sample size and the deviation parameter a. For larger deviations, $a = 3m/4$ and $a = m/2$, the test shows high power even for smaller sample sizes, $m = 50$. As the expected sample size increases to $m = 100$ and beyond, the test achieves near-perfect power for these deviations. For the smallest deviation, $a = m/4$, the power is moderate for small expected sample sizes, but improves substantially with larger sample sizes. Table 4 presents similar results with power increasing with both the expected sample size and the deviation parameter a. However, the test presents lower power values across all sample sizes and deviation parameters for *Dendrite* compared to *Spiders*. Despite this, the Kolmogorov–Smirnov type test statistic shows high power and a good overall performance.

Cramér von Mises type test statistic

Although the Cramér von Mises type test statistic does not depend on whether or not the network is a tree, for consistency with what it has been previously done, we study its performance for both *Spiders* and *Dendrite* networks.

The high number of nodes of the proposed networks makes it computationally challenging to run our simulation study without significant benefits to understanding the testing procedures. Therefore, to reduce computational costs while maintaining the nature of the networks, we consider "subnetworks" of *Spiders* and *Dendrite* for our scenarios. These subnetworks are derived by limiting ourselves to a subset (in the Euclidean plane) of the original graphs. Although these subnetworks have fewer nodes, they still represent the corresponding geometric structures. For instance, the subnetwork of *Spiders* retains cycles, and the subnetwork of *Dendrite* remains a tree. Additionally, the number of permutations is reduced to $n_p = 5000$, a choice that, according to Marozzi (2004), does not compromise the calibration process. Figure 7 shows the representation of these subnetworks.

The same homogeneous and inhomogeneous intensities, as defined in (9) and (10), have been considered, but limited to the corresponding subnetworks. The resulting relative density functions in the subnetworks are represented in Fig. 8.

The results presented in Tables 5 and 6 illustrate that the Cramér von Mises type test statistic exhibits a good level adjustment across both network models. Table 5 shows that the observed rejection proportions are close to the nominal levels for $m \geq 100$ with slightly higher values for the inhomogeneous model in most sample sizes and significance levels. The rejection proportions for *Dendrite*, see Table 6, seems higher

than in *Spiders* and present almost perfect adjustment for $m \geq 50$. Even for smaller expected sample sizes, $m = 20$, the values are quite competitive.

To analyse the power of this proposal we follow the approach outlined in Sect. 4.2, but applied to the subnetworks. Specifically, the subsets $\mathcal{L}_{\mathcal{G}}^{+}$ in which a number a of expected points are added homogeneously are defined as follows:

$$\mathcal{L}_{SubSpiders}^{+} = \left\{ \boldsymbol{p} \in \mathcal{L}_{SubSpiders} \colon \boldsymbol{p} \in [735.25,\ 984.375] \times [735.25,\ 956.25] \right\}, \quad (14)$$

and

$$\mathcal{L}_{SubDendrite}^{+} = \{ \boldsymbol{p} = (p_1, p_2) \in \mathcal{L}_{SubDendrite} \colon p_2 > 295.9625 \}. \quad (15)$$

These choices ensure that the ratio $|\mathcal{L}_{\mathcal{G}}^{+}|/|\mathcal{L}_{\mathcal{G}}|$ is approximately the same for both networks. The representations of these intensity functions are shown in Fig. 9 (homogeneous) and Fig. 10 (inhomogeneous).

Tables 7 and 8 present the proportions of rejections for different alternative hypotheses (controlled by the deviation parameter a) using the Cramér von Mises type test statistic on the subnetworks of *Spiders* and *Dendrite*, respectively. Note that same values of a apply to both subnetworks.

In both scenarios, Tables 7 and 8, the power of the test statistic increases with the parameter a for a fixed sample size, and similarly increases with the sample size for a fixed a. This trend is consistent across both homogeneous and inhomogeneous models. Notably, even when the deviation from the null hypothesis is relatively small, $a = m/4$, the test still achieves high power values indicating a very good performance of this proposal.

It is important to note that the simulation results discussed so far assume a balanced scenario, where the expected number of points in the two simulated patterns is the same. However, this balanced condition may not always be realistic. Practitioners may encounter

significantly unbalanced point patterns, where the numbers of events differ by several orders of magnitude. To address this, we have also considered two unbalanced scenarios, specifically $m_1 = 2m_2$ and $m_1 = 4m_2$. Detailed results for these unbalanced

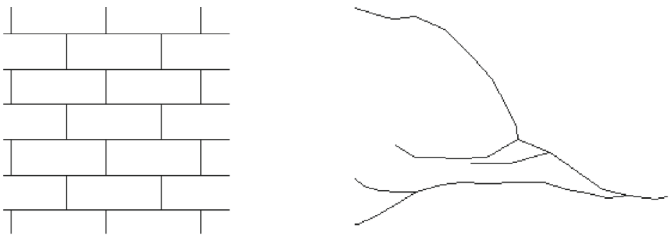

(a) Subnetwork of *Spiders*.

(b) Subnetwork of *Dendrite*.

Fig. 7 Representation of the subnetworks of *Spiders* and *Dendrite* used in the analysis of the Cramér von Mises type test statistic

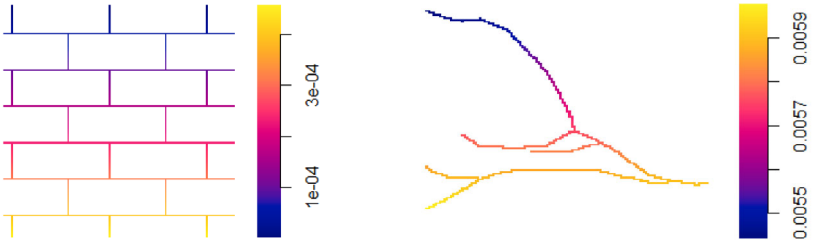

(a) Subnetwork of *Spiders*. (b) Subnetwork of *Dendrite*.

Fig. 8 Relative density functions associated with the inhomogeneous model for both, the subnetwork of *Spiders* and *Dendrite*

Table 5 Proportion of rejections under the null hypothesis for the Cramér von Mises type test statistic on the subnetwork of *Spiders*, for both the homogeneous and inhomogeneous models

	Homogeneous model			Inhomogeneous model		
	$\alpha = 0.1$	$\alpha = 0.05$	$\alpha = 0.01$	$\alpha = 0.1$	$\alpha = 0.05$	$\alpha = 0.01$
$m = 20$	0.077	0.035	0.001	0.073	0.026	0.002
$m = 50$	0.076	0.037	0.005	0.087	0.038	0.004
$m = 100$	0.080	0.046	0.002	0.097	0.050	0.011
$m = 200$	0.107	0.044	0.003	0.098	0.051	0.006
$m = 500$	0.090	0.043	0.013	0.092	0.047	0.008
$m = 750$	0.101	0.044	0.009	0.081	0.038	0.008

Table 6 Proportion of rejections under the null hypothesis for the Cramér von Mises type test statistic on the subnetwork of *Dendrite*, for both the homogeneous and inhomogeneous models

	Homogeneous model			Inhomogeneous model		
	$\alpha = 0.1$	$\alpha = 0.05$	$\alpha = 0.01$	$\alpha = 0.1$	$\alpha = 0.05$	$\alpha = 0.01$
$m = 20$	0.086	0.042	0.005	0.089	0.045	0.007
$m = 50$	0.091	0.040	0.006	0.088	0.048	0.003
$m = 100$	0.108	0.048	0.003	0.084	0.041	0.011
$m = 200$	0.099	0.039	0.013	0.100	0.048	0.010
$m = 500$	0.106	0.040	0.005	0.102	0.037	0.003
$m = 750$	0.089	0.048	0.008	0.098	0.048	0.008

scenarios, which are as satisfactory as those in the balanced case, can be found in Appendix A.1 and A.2, respectively.

4.4 The effect of the network

It has been proved along the last decades that the use of linear networks is required when analysing point processes with this domain, and that the straightforward application of spatial point process methodology to point processes on linear networks is not an

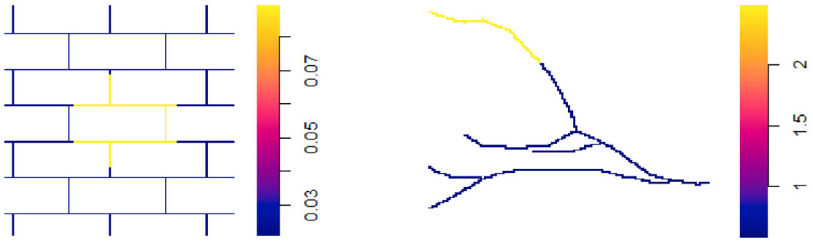

(a) Subnetwork of *Spiders*. (b) Subnetwork of *Dendrite*.

Fig. 9 For $m = 100$ and $a = 50$, representation of the perturbed homogeneous intensity function according to (11) in both subnetworks

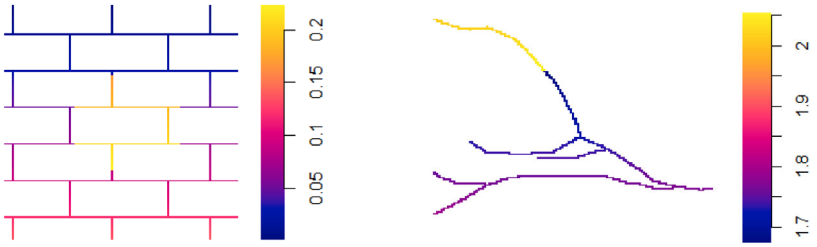

(a) Subnetwork of *Spiders*. (b) Subnetwork of *Dendrite*.

Fig. 10 For $m = 300$, $a_{SubSpiders} = 100$ and $a_{SubDebdrite} = 10$ representation of the perturbed inhomogeneous intensity function according to (11) in both subnetworks

appropriate choice. For instance, Okabe and Sugihara (2012) state that 'originally, planar spatial methods were designed for analysing events on a plane, but in practice, as a matter of convenience, planar spatial methods were often applied to network events. However, this use is likely to lead to false conclusions'.

In our scenario, the network has varying degrees of involvement depending on whether we are working with the Kolmogorov–Smirnov type test statistic or the Cramér von Mises one. In the former, the selection of the π-system is very different from what it would be done for planar point processes. Moreover, when estimating the normalizing constant ξ, we use a partition of the network into its edges, i.e., a natural partition of a linear network which does not directly extend to the plane. Regarding the Cramér von Mises type test statistic, the role of the linear network comes when estimating the intensity functions. As detailed in Okabe and Sugihara (2012), Baddeley et al. (2015) and McSwiggan et al. (2017) among others, the network structure must be considered when estimating the intensity function of a point process on a linear network to obtain consistent and unbiased estimates.

Moreover, the network has an important effect in the testing procedures presented in this paper. We have rerun the simulations previously presented but omitting the network structure, i.e., patterns are generated on the network, but then the spatial version of the test statistics developed in Fuentes-Santos et al. (2023) were applied. The results show that for both, *Spiders* and *Dendrite* the level values are slightly lower but not so far apart from the correct ones. However, an important decrease in power

Table 7 Proportion of rejections for different alternative hypotheses (deviation from the null hypothesis controlled by parameter a) for the Cramér von Mises type test statistic on the subnetwork of *Spiders*, for both homogeneous and inhomogeneous models

	Homogeneous model			Inhomogeneous model		
	$a = 3m/4$	$a = m/2$	$a = m/4$	$a = 3m/4$	$a = m/2$	$a = m/4$
$m = 50$	0.873	0.557	0.168	0.905	0.612	0.184
$m = 100$	0.999	0.927	0.378	1	0.926	0.414
$m = 200$	1	1	0.790	1	0.999	0.738
$m = 500$	1	1	0.994	1	1	0.999

Table 8 Proportion of rejections for different alternative hypotheses (deviation from the null hypothesis controlled by parameter a) for the Cramér von Mises type test statistic on the subnetwork of *Dendrite*, for both homogeneous and inhomogeneous models

	Homogeneous model			Inhomogeneous model		
	$a = 3m/4$	$a = m/2$	$a = m/4$	$a = 3m/4$	$a = m/2$	$a = m/4$
$m = 50$	0.977	0.843	0.377	0.985	0.848	0.394
$m = 100$	1	0.986	0.669	1	0.992	0.680
$m = 200$	1	1	0.938	1	1	0.994
$m = 500$	1	1	1	1	1	1

values appears, specially for the *Dendrite* network. We do not expect a significant difference in *Spiders* due to its grid-like geometry. Note that the effect of the network highly depends on its geometry, and when there is a network almost covering the planar region in which it is embedded, the shortest-path distance and the euclidean distance values are similar. Hence, it is quite natural that for 'more dense' networks the use of planar point processes methodology and specifically designed one shows fewer differences.

5 Analysing traffic accidents in Rio de Janeiro

Road safety has been a general interest in societies worldwide over the past century. Stricter driving regulations have been implemented, awareness of driving dangers and responsibilities has increased, manuals on pedestrian safety have been developed... The main aim of all these efforts is to reduce road-related mortality rates.

Traffic accidents are currently estimated to be the eighth leading cause of death across all age groups, and are predicted to become the seventh leading cause of death by 2030, see WHO (2023). Consequently, this problem is widely studied from different perspectives in almost every country. For instance, Bacchieri and Barros (2011) discusses the increase in the absolute number of deaths and in the mortality rates in Brazil; Gopalakrishnan (2012) does the same for India; Ghadirzadeh et al. (2015) reports that even though the mortality of traffic accidents in Iran has decreased in the recent years, it is still alarmingly high; and Yang and Kim (2003) analyses dif-

Table 9 Example of one entry of the database with the available information

Street: Rodrigues Alves avenue	
Time: 2019-10-16 21:35:08 UTC	
Lat: −22.892743	Lon: −43.19547
Type: Accident	Subtype: Major accident
Road type: 2	Reliability: 7
Magvar: 267	Reports ratings: 3

ferent causes of the (also high) mortality rates in Korea over the last decades. The statistical aspects of traffic mortality have also been the subject of intense research in many different fields, not only from the perspective of point processes on linear networks. McSwiggan (2019) applies relative risk estimation based on kernel methods on linear networks to the Geelong road accidents data set, and Moradi and Mateu (2020) use their first- and second-order characteristics of spatio-temporal point processes on networks to the study of traffic accidents in three different cities worldwide. Additionally, Briz-Redón et al. (2019) uses a conditional autoregressive (CAR) model with a negative binomial response to estimate the occurrence of traffic accidents near school locations, and Zheng et al. (2024) uses spatial regression models based on a geostatistical approach.

The estimation of the distribution of traffic accidents on a road network, the identification of points with the greatest accumulation of accidents (black spots), and the elements that impact them are essential tasks to improve road safety and, hence, save lives. The city council of Rio de Janeiro has launched a project to improve road safety in the city and its surroundings. The project's aim is to attain safer streets for everyone in Rio de Janeiro and prevent every crash on the streets, as this is the next step to a safer, more vibrant future.

As a result of this project, a data set of traffic accidents in Rio de Janeiro has been provided. The database has 270908 entries, each corresponding to a traffic accident on a road in Rio de Janeiro between March 21st, 2019 and May 4th, 2022. These events are reported by a driver or a passer-by via Waze.[1] For each event, the following information is reported: **Street**, the name of the street in Rio de Janeiro where the accident took place; **Time**, date and time at which the event was reported; **Latitude** and **longitude**, geographical coordinates of the reported accident; **Type**, the type of event reported (in our database this information is redundant, as all the entries represent traffic accidents); **Subtype**, giving more detailed information about the type of accident reported (whether it was a major or minor accident); **Road type**, numerical code indicating the type of road in which the accident took place (code 2 used in Table 9 indicates "Primary Street"); **Magvar**, direction in which the driver was headed at the time of the accident, understood as an angle (integer between 0 and 359, understanding 0 pointing north); **ReportRating**, rank of the user reporting the accident (an integer from 1 to 6, 6 being the highest score); **Reliability**, confidence score (integer between 0 and 10) given to the report based on other users' input and the ReportRating. Table 9 shows an example of a database entry.

[1] The main site of this platform can be accessed through: https://www.waze.com/en/live-map

(a) Map of the main roads of Rio de Janeiro extracted from Google (2022).

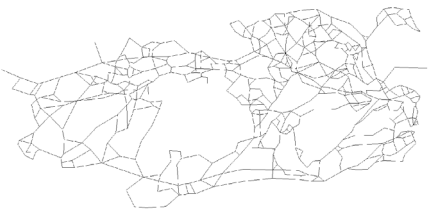

(b) Linear network representing the main road network of Rio de Janeiro.

Fig. 11 Map of the main roads of Rio de Janeiro (**a**), and the associated linear network (**b**)

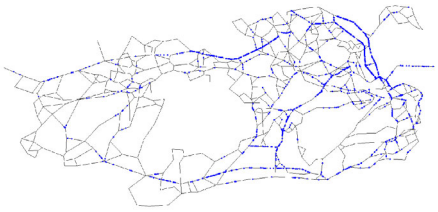

(a) Morning rush hour with 1439 events.

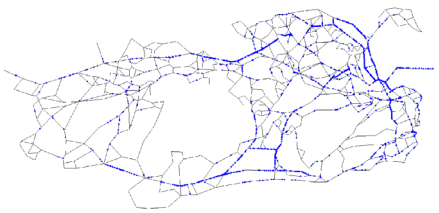

(b) Afternoon rush hour with 1857 events.

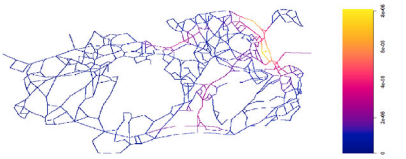

(c) Intensity estimation for the morning rush hour.

(d) Intensity estimation for the afternoon rush hour.

Fig. 12 Representation on the linear network with the traffic accidents which happened on main roads in the year 2021 with a maximum Reliability report between 11 and 12 h (**a**), and between 21 and 22 h, (**b**). Furthermore, estimators of the relative density of the point processes associated with these point patterns have been represented on a common scale in (**c**) and (**d**), respectively

We are interested in analysing the distribution of traffic accidents along the road network of Rio de Janeiro. Particularly we address the problem of comparing the traffic accident distribution between the morning and evening rush hours around the city.

To approach this problem using our previously presented tools, a linear network needs to be defined. Since the majority of accidents in Rio occur on main roads, we decided to consider only those. Therefore, the map of Rio de Janeiro, shown in Fig. 11a, was used as a reference. The nodes of the linear network represent the road intersections, and the edges represent the roads connecting these intersections. We approximate by considering straight roads instead of curved ones, which introduces minimal error due to the high number of intersections.

The coordinates of the network are in latitude-longitude format. To accurately analyse this, we apply the Universal Transverse Mercator (UTM) projection, specifically UTM Zone 23 S. The linear network depicted in Fig. 11b is obtained.

The accidents' locations in our database are also in latitude-longitude format, so the UTM projection needs to be applied to them as well. Since our approximation of the Rio de Janeiro road map represents curved roads as straight lines, accidents may not fall exactly on the network. To address this, we use the *spatstat* package Baddeley et al. (2015), which replaces each accident with the nearest point on the network, producing minimal error that remains within acceptable limits.

To ensure data quality, we only consider accidents reported with the highest Reliability score. Rush hours have been defined based on expert knowledge and data analysis, resulting in 11-12 am and 9-10pm being selected as the morning and evening rush hours, respectively. These two point patterns are represented on the linear network in Fig. 12a, b. The density estimation of the point processes is also computed and shown in Fig. 12c, d. These estimators were performed using the heat equation estimator by McSwiggan et al. (2017), with the bandwidth determined by a modified Scott's rule.

To compare the traffic accident distribution on Rio de Janeiro's roads between the morning and evening rush hours, we use the Kolmogorov–Smirnov and the Cramér von Mises type test statistics, both using 10000 permutations. Both procedures were defined and tested under a Poisson assumption. As noted in Remark 2, few tools exist to test if a point pattern on a linear network follows an inhomogeneous Poisson point process.

To mitigate this drawback, we employed a procedure inspired by Loosmore and Ford (2006). The approach involves selecting a function describing interaction, simulating multiple realizations under the hypothesis of interest, in our case, an inhomogeneous Poisson process, and then computing the function for each realization. An envelope is defined by taking the point-wise maximum and minimum of these simulated functions, as suggested in Ripley (1977). As explained in Baddeley et al. (2014), global envelopes should only be used for exploratory purposes. Therefore, to rigorously test the hypothesis of interest, a formal statistical test should be conducted.

There are several options for functions that describe interaction: the K-function, the L-function or the pair correlation function. Okabe and Yamada (2001) and Ang et al. (2012) adapted the K-function and pair correlation function to point patterns on linear networks. We chose to use the K-function and to run 2500 Monte Carlo simulations following the recommendations in Myllymaki et al. (2017). We then conducted a DCLF test, which uses as its statistic the quadratic distance between the observed K-function and the K-function under the null hypothesis, estimated as the point-wise mean of all simulated K-functions within the envelope; see Loosmore and Ford (2006) and Baddeley et al. (2014) for details. The resulting p-values are 0.417 and 0.2631 for the morning and evening rush hours, respectively. Thus, the Poisson hypothesis is not rejected in either case.

The Kolmogorov–Smirnov test resulted in a p-value of 0.6315, while the Cramér von Mises test produced a p-value of $5 \cdot 10^{-5}$. This discrepancy indicates that the two tests do not provide compatible results. Several factors could contribute to this difference. The Kolmogorov–Smirnov test aggregates discrepancies, unlike the Cramér von Mises test, similar to the differences between Lilliefors and Shapiro-Wilks tests for Gaussian distribution. This issue has been discussed in mean regression goodness-of-fit tests by Horowitz and Spokoiny (2001).

Additionally, this is a preliminary approach to comparing populations in point processes on linear networks, and we have not conducted a sensitivity analysis regarding various choices for each test: the partition, the π-system, and its base node for the Kolmogorov–Smirnov test, or the type of nonparametric estimator and its bandwidth parameter for the Cramér von Mises test.

Furthermore, considering the data's nature, there may be accident black spots in Rio de Janeiro's road network. These "peaks of incidence" might go unnoticed by the Kolmogorov–Smirnov test, leading to the assumption that the intensity of accidents during both rush hours is similar, while the Cramér von Mises test clearly rejects this null hypothesis.

6 Conclusions and discussions

The problem of testing whether two point processes share the same spatial structure had already been studied in the euclidean plane, however, no developments have been made in the context of point processes on linear networks.

In this work, we have proposed two methods to test proportionality of first-order intensity functions for Poisson point processes on linear networks, which is equivalent to testing their spatial structure. To tackle this problem two different methodologies were proposed: a Kolmogorov–Smirnov and a Cramér von Mises type test statistic, whose good performance in finite samples is shown in an extensive simulation study. Both tests provide with a very good level adjustment, even for small expected sample sizes, and they both reach high power values at alternatives not so far from the null hypothesis. In this latter scenario, the Cramér von Mises type test statistic seems better at detecting the deviations from the null hypothesis. Equally satisfactory results have also been obtained in unbalanced situations, i.e., when the expected sample sizes of each pattern are different.

We also applied our new proposals to a very interesting data set of traffic accidents in Rio de Janeiro (Brazil). Particularly we tested whether the traffic accidents in the morning rush hour have the same spatial structure than those occurring during the evening rush hour. Unfortunately, looking at the results of both test statistics we could not find a common answer to that question, i.e., the Kolmogorov–Smirnov type test statistic does not detect any difference while the Cramér von Mises type one clearly rejects the null hypothesis of proportional intensity functions. As we have discussed in detail in Sect. 5, there might be different factors underlying these results, such as the different choices (with no optimal procedure established thus far) that need to be made in every test, or the particular structure of the data with very small regions with high incidence of traffic accidents (black-spots) that may not be detected by the Kolmogorov–Smirnov type test statistic.

This work is intended to be a preliminary step in addressing such testing problems for point processes on linear networks. Consequently, several future research directions have been identified. One essential development is the derivation of the asymptotic distribution of these test statistics, either for direct use (if a good convergence rate is achieved) or to define a specifically adapted bootstrap scheme, which could be a competitive alternative to the current permutation-based calibration. This

could significantly reduce the computational cost, which is a crucial challenge for point processes on linear networks. Additionally, the development of bandwidth selection methods for testing purposes remains an open problem in the general nonparametric context, particularly for point processes. Defining appropriate selectors could enhance the results.

Another intriguing but complex issue is comparing the spatial structure of non-Poisson point processes. The assumption of Poisson processes may be too restrictive in some situations where interactions between points exist. The definition of other types of point processes on linear networks is still limited and recent, see D'Angelo et al. (2022) for Gibbs point processes and Møller and Rasmussen (2024) for Cox processes. Moreover, the main challenge in this generalisation could be that the null hypothesis, as stated in (2), might not be well-defined in a more general context, which means that more information should be included in the definition of the problem. Also, because of this, permutations might not be consistent as a way to calibrate those test statistics. A possible way to overcome this issue might be the use of robust permutation tests based on studentized test statistics, see Bertanha and Chung (2023). However, note that studentization of some statistics might be analytically complicated and computationally burdensome. Hence some research is needed to be able to fully generalise our procedures in an appropriate way to non-Poisson point processes.

Lastly, we want to point out that the methods proposed in this paper are not only a first step in addressing the classical two-sample problem for point processes on linear networks, but they are also an essential element for the future development of classification techniques. Assume we have several patterns over the same linear network, such as traffic accidents in the same city involving different types of vehicles, or with varying degrees of consequences (minor injuries, major injuries, deaths...). An interesting problem is determining which of those patterns are generated by the same underlying process, and how many different processes exist. The idea is to adapt to point processes on linear networks the concepts presented in Khismatullina and Vogt (2023) to classify intensity functions for temporal point processes, which rely on the existence of an appropriate two-sample test in the context of interest, driven into a multi-scale approach.

Supplementary information.

Supplementary material related to this article has been provided with the submission.

Appendix A Unbalanced simulation study

In our simulation study, the results of which are presented in Sect. 4.3, we only consider the balanced scenario, i.e., we use equal expected sample sizes for the two processes involved in the testing problem. However, as previously mentioned, this condition may not always be the case for real data applications. Hence, we present here the results of an analogous simulation study, but with different expected sample sizes for the compared point processes.

An important question arises for the power study in the unbalanced scenario: which of the two point processes should have its intensity perturbed as in Eq. (11)? The one with the larger or smaller expected number of events? As there is no clear preference, we performed the power study for both. Another consideration is the degree of imbalance in the expected sample sizes. We consider two cases: $m_1 = 2m_2$, see Sect. A.1, and $m_1 = 4m_2$, see Sect. A.2.

A.1 Unbalanced simulation study: $m_1 = 2m_2$

Kolmogorov–Smirnov type statistic

To study the level adjustment, we proceed in a manner similar to that detailed in Sect. 4.3. We consider two networks, *Spiders* and *Dendrite*, with base points for the π-systems as shown in Fig. 6. Additionally, we consider both homogeneous and inhomogeneous intensity functions, as detailed in (9) and (10).

Tables 10 and 11 present the rejection proportions under the null hypothesis for the Kolmogorov–Smirnov type test statistic applied to the *Spiders* network. The proportions are computed for different significance levels, α, and are reported for both homogeneous and inhomogeneous models, across varying sample sizes. These tables show that the Kolmogorov–Smirnov type test statistic performs well in controlling type I error for expected sample sizes $m_2 = 100 = m_1/2$ in both homogeneous and

Table 10 Proportion of rejections under the null hypothesis for the Kolmogorov–Smirnov type test statistic on *Spiders*

		Homogeneous model			Inhomogeneous model		
m_1	m_2	$\alpha = 0.1$	$\alpha = 0.05$	$\alpha = 0.01$	$\alpha = 0.1$	$\alpha = 0.05$	$\alpha = 0.01$
40	20	0.114	0.063	0.013	0.084	0.037	0.007
100	50	0.104	0.050	0.018	0.099	0.056	0.009
200	100	0.086	0.037	0.006	0.103	0.061	0.014
400	200	0.079	0.040	0.003	0.097	0.061	0.012
1000	500	0.101	0.045	0.008	0.104	0.057	0.016
1500	750	0.115	0.060	0.017	0.096	0.053	0.004

Table 11 Proportion of rejections under the null hypothesis for the Kolmogorov–Smirnov type test statistic on *Dendrite*

		Homogeneous model			Inhomogeneous model		
m_1	m_2	$\alpha = 0.1$	$\alpha = 0.05$	$\alpha = 0.01$	$\alpha = 0.1$	$\alpha = 0.05$	$\alpha = 0.01$
40	20	0.097	0.056	0.012	0.088	0.047	0.007
100	50	0.105	0.057	0.015	0.108	0.049	0.011
200	100	0.101	0.055	0.012	0.098	0.058	0.010
400	200	0.086	0.046	0.006	0.100	0.041	0.004
1000	500	0.107	0.056	0.014	0.127	0.068	0.011
1500	750	0.104	0.057	0.010	0.099	0.049	0.010

inhomogeneous models, and the deviation is almost acceptable for smaller expected sample sizes such as $m_2 = 50 = m_1/2$.

Let us now focus on the power of the Kolmogorov–Smirnov type test statistic. In both the homogeneous and inhomogeneous cases, the intensity is perturbed as detailed in Eq. (11), using the same subregions for perturbation as specified in the balanced case, see Eq. (12) for *Spiders* and Eq. (13) for *Dendrite*. For the unbalanced scenarios, we follow this convention: the process with unperturbed intensity has m_1 expected points, while the perturbed process has $m_2 + a$ expected points.

Table 12 Proportion of rejections for different alternative hypotheses (deviation from the null hypothesis controlled by parameter a) for the Kolmogorov–Smirnov type test statistic on *Spiders*

		Homogeneous model			Inhomogeneous model		
m_1	m_2	$a = 3m_2/4$	$a = m_2/2$	$a = m_2/4$	$a = 3m_2/4$	$a = m_2/2$	$a = m_2/4$
100	50	0.986	0.869	0.396	0.996	0.927	0.450
200	100	1	0.994	0.681	1	0.999	0.736
400	200	1	1	0.937	1	1	0.974
1000	500	1	1	1	1	1	1

Table 13 Proportion of rejections for different alternative hypotheses (deviation from the null hypothesis controlled by parameter a) for the Kolmogorov–Smirnov type test statistic on *Dendrite*

Homogeneous model					
m_1	m_2	a=$7m_2/4$	$a = 3m_2/2$	$a = 5m_2/4$	$a = m_2$
100	50	0.636	0.578	0.478	0.375
200	100	0.958	0.913	0.859	0.730
400	200	1	1	0.999	0.982
1000	500	1	1	1	1
Inhomogeneous model					
100	50	0.630	0.576	0.489	0.369
200	100	0.951	0.899	0.831	0.711
400	200	1	1	0.997	0.980
1000	500	1	1	1	1

Table 14 Proportion of rejections for different alternative hypotheses (deviation from the null hypothesis controlled by parameter a) for the Kolmogorov–Smirnov type test statistic on *Spiders*

		Homogeneous model			Inhomogeneous model		
m_1	m_2	$a = 3m_2/4$	$a = m_2/2$	$a = m_2/4$	$a = 3m_2/4$	$a = m_2/2$	$a = m_2/4$
50	100	0.954	0.776	0.315	0.984	0.867	0.436
100	200	1	0.985	0.622	1	0.995	0.735
200	400	1	1	0.918	1	1	0.966
500	1000	1	1	0.999	1	1	1

Table 15 Proportion of rejections for different alternative hypotheses (deviation from the null hypothesis controlled by parameter a) for the Kolmogorov–Smirnov type test statistic on *Dendrite*

Homogeneous model					
m_1	m_2	a=$7m_2/4$	$a = 3m_2/2$	$a = 5m_2/4$	$a = m_2$
50	100	0.291	0.268	0.243	0.214
100	200	0.577	0.562	0.523	0.452
200	400	0.950	0.935	0.876	0.812
500	1000	1	1	1	1
Inhomogeneous model					
50	100	0.318	0.317	0.270	0.231
100	200	0.609	0.560	0.545	0.452
200	400	0.940	0.919	0.881	0.797
500	1000	1	1	1	1

Table 12 shows the proportion of rejections for various alternative hypotheses (with deviations from the null controlled by a) in *Spiders*, for both homogeneous and inhomogeneous models. A similar summary for *Dendrite* is presented in Table 13. In Tables 14 and 15 the same results are shown when perturbing the process with the smaller expected sample size.

In Tables 12, 13, 14 and 15 we observe a similar behaviour to that seeen in the balanced scenario. The power increases with a for all expected sample sizes, as the deviation from the null hypothesis becomes more pronounced. Additionally, for a fixed ratio a/m_2, the power increases rapidly with m_2 reflecting the benefit of having more information about the process.

Cramér von Mises type test statistic

To study the level adjustment of the Cramér von Mises type test statistic in an unbalanced scenario, we proceed similarly to Sect. 4.3. We consider the subnetworks of *Spiders* and *Dendrite* introduced in Fig. 7. On these subnetworks, we define both homogeneous and inhomogeneous models as detailed in (9) and (10), respectively.

Table 16 presents the proportion of rejections for different expected sample sizes, specifically $m_1 = 2m_2$, and for different nominal significance levels, α in the subnetwork of *Spiders*. A similar summary for the subnetwork of *Dendrite* is provided in

Table 16 Proportion of rejections under the null hypothesis for the Cramér von Mises type test statistic on the subnetwork of *Spiders*

		Homogeneous model			Inhomogeneous model		
m_1	m_2	$\alpha = 0.1$	$\alpha = 0.05$	$\alpha = 0.01$	$\alpha = 0.1$	$\alpha = 0.05$	$\alpha = 0.01$
20	40	0.065	0.02	0.004	0.092	0.040	0.005
50	100	0.079	0.031	0.006	0.088	0.035	0.004
100	200	0.069	0.037	0.007	0.089	0.042	0.011
200	400	0.098	0.045	0.003	0.094	0.048	0.012
500	1000	0.101	0.048	0.013	0.077	0.040	0.008
750	1500	0.101	0.055	0.007	0.091	0.037	0.005

Table 17. Both these tables indicate that, even in this unbalanced scenario, the Cramér von Mises type statistic is well calibrated for $m_1 = m_2/2 \geq 200$, in both homogeneous and inhomogeneous models.

Finally, we focus on the power of the Cramér von Mises type statistic. For the models under the alternative hypothesis, we perturb the intensity function as described in Eq. (11), using the same perturbation subregions as in the balanced case, detailed in (14) for the subnetwork of *Spiders* and in (14) for the subnetwork of *Dendrite*. Additionally, we use the same convention for the unbalanced nature of the expected number of points as applied to the Kolmogorov–Smirnov type statistic.

Table 18 presents the proportion of rejections for different possible alternative hypotheses (deviation from the null controlled by a) in the subnetwork of *Spiders*, for both homogeneous and inhomogeneous models. An analogous summary for the

Table 17 Proportion of rejections under the null hypothesis for the Cramér von Mises type test statistic on the subnetwork of *Dendrite*

		Homogeneous model			Inhomogeneous model		
m_1	m_2	$\alpha = 0.1$	$\alpha = 0.05$	$\alpha = 0.01$	$\alpha = 0.1$	$\alpha = 0.05$	$\alpha = 0.01$
20	40	0.109	0.055	0.010	0.112	0.059	0.010
50	100	0.095	0.059	0.011	0.085	0.043	0.009
100	200	0.098	0.049	0.009	0.097	0.046	0.009
200	400	0.092	0.054	0.014	0.097	0.051	0.014
500	1000	0.115	0.053	0.004	0.105	0.050	0.008
750	1500	0.096	0.047	0.007	0.097	0.050	0.008

Table 18 Proportion of rejections for different alternative hypotheses (deviation from the null hypothesis controlled by parameter a) for the Cramér von Mises type test statistic on the subnetwork of *Spiders*

		Homogeneous model			Inhomogeneous model		
m_1	m_2	$a = 3m_2/4$	$a = m_2/2$	$a = m_2/4$	$a = 3m_2/4$	$a = m_2/2$	$a = m_2/4$
100	50	0.981	0.792	0.294	0.974	0.798	0.311
200	100	1	0.990	0.599	1	0.981	0.551
400	200	1	1	0.918	1	1	0.897
1000	500	1	1	1	1	1	1

Table 19 Proportion of rejections for different alternative hypotheses (deviation from the null hypothesis controlled by parameter a) for the Cramér von Mises type test statistic on the subnetwork of *Dendrite*

		Homogeneous model			Inhomogeneous model		
m_1	m_2	$a = 3m_2/4$	$a = m_2/2$	$a = m_2/4$	$a = 3m_2/4$	$a = m_2/2$	$a = m_2/4$
100	50	0.997	0.933	0.497	0.997	0.941	0.494
200	100	1	0.998	0.805	1	0.999	0.822
400	200	1	1	0.984	1	1	0.987
1000	500	1	1	1	1	1	1

Table 20 Proportion of rejections for different alternative hypotheses (deviation from the null hypothesis controlled by parameter a) for the Cramér von Mises type test statistic on the subnetwork of *Spiders*

		Homogeneous model			Inhomogeneous model		
m_1	m_2	$a = 3m_2/4$	$a = m_2/2$	$a = m_2/4$	$a = 3m_2/4$	$a = m_2/2$	$a = m_2/4$
50	100	0.967	0.754	0.244	0.975	0.770	0.273
100	200	1	0.983	0.529	1	0.987	0.538
200	400	1	1	0.910	1	1	0.896
500	1000	1	1	0.999	1	1	1

Table 21 Proportion of rejections for different alternative hypotheses (deviation from the null hypothesis controlled by parameter a) for the Cramér von Mises type test statistic on the subnetwork of *Dendrite*

		Homogeneous model			Inhomogeneous model		
m_1	m_2	$a = 3m_2/4$	$a = m_2/2$	$a = m_2/4$	$a = 3m_2/4$	$a = m_2/2$	$a = m_2/4$
50	100	0.996	0.931	0.507	0.995	0.935	0.506
100	200	1	0.999	0.810	1	0.999	0.830
200	400	1	1	0.981	1	1	0.988
500	1000	1	1	1	1	1	1

subnetwork of *Dendrite* is shown in Table 19. Tables 20 and 21 show the same results when the process with the smaller expected number of observed points is perturbed.

In Tables 18, 19, 20 and 21 we observe similar behaviour to that in the balanced case: for all expected sample sizes, power increases with a s we move further from the null hypothesis. Moreover, for a fixed ratio a/m_2, power also increases rapidly with m_2.

A.2 Unbalanced simulation study: $m_1 = 4m_2$

The results here are analogous to those in Sect. A.1, but with $m_1 = 4m_2$. Similar observations to those previously detailed apply here.

Kolmogorov–Smirnov type test statistic

See Tables 22, 23, 24, 25, 26, 27, 28, 29, 30, 31, 32, and 33.

We observe that both the level adjustment and power values for the Kolmogorov–Smirnov type test statistic yield satisfactory results, similar to those obtained with $m_1 = 2m_2$.

Cramér von Mises type test statistic

We observe that both the level adjustment and power values for the Cramér von Mises type test statistic yield satisfactory results, similar to those obtained with $m_1 = 2m_2$.

Table 22 Proportion of rejections under the null hypothesis for the KS type test statistic on *Spiders*

		Homogeneous model			Inhomogeneous model		
m_1	m_2	$\alpha = 0.1$	$\alpha = 0.05$	$\alpha = 0.01$	$\alpha = 0.1$	$\alpha = 0.05$	$\alpha = 0.01$
80	20	0.104	0.058	0.016	0.091	0.042	0.016
200	50	0.098	0.055	0.014	0.101	0.042	0.007
400	100	0.087	0.037	0.002	0.116	0.056	0.015
800	200	0.092	0.041	0.007	0.095	0.052	0.016
2000	500	0.101	0.050	0.015	0.111	0.056	0.009

Table 23 Proportion of rejections under the null hypothesis for the KS type test statistic on *Dendrite*

		Homogeneous model			Inhomogeneous model		
m_1	m_2	$\alpha = 0.1$	$\alpha = 0.05$	$\alpha = 0.01$	$\alpha = 0.1$	$\alpha = 0.05$	$\alpha = 0.01$
80	20	0.094	0.046	0.008	0.105	0.050	0.009
200	50	0.105	0.048	0.012	0.110	0.049	0.006
400	100	0.109	0.047	0.008	0.099	0.047	0.010
800	200	0.089	0.051	0.008	0.099	0.047	0.010
2000	500	0.112	0.059	0.010	0.100	0.054	0.013

Table 24 Proportion of rejections for different alternative hypotheses (deviation from the null hypothesis controlled by parameter a) for the KS type test statistic on *Spiders*

		Homogeneous model			Inhomogeneous model		
m_1	m_2	$a = 3m_2/4$	$a = m_2/2$	$a = m_2/4$	$a = 3m_2/4$	$a = m_2/2$	$a = m_2/4$
200	50	0.999	0.935	0.477	1	0.964	0.436
400	100	1	0.997	0.775	1	0.998	0.808
800	200	1	1	0.989	1	1	0.968
2000	500	1	1	1	1	1	1

Table 25 Proportion of rejections for different alternative hypotheses (deviation from the null hypothesis controlled by parameter a) for the KS type test statistic on *Spiders*

		Homogeneous model			Inhomogeneous model		
m_1	m_2	$a = 3m_2/4$	$a = m_2/2$	$a = m_2/4$	$a = 3m_2/4$	$a = m_2/2$	$a = m_2/4$
50	200	0.954	0.809	0.353	0.984	0.893	0.485
100	400	1	0.989	0.680	1	0.988	0.799
200	800	1	1	0.956	1	1	0.984

Table 26 Proportion of rejections for different alternative hypotheses (deviation from the null hypothesis controlled by parameter a) for the KS type test statistic on *Dendrite*

Homogeneous model					
m_1	m_2	a=$7m_2/4$	$a = 3m_2/2$	$a = 5m_2/4$	$a = m_2$
200	50	0.889	0.801	0.674	0.533
400	100	0.999	0.990	0.967	0.884
800	200	1	1	1	0.999
Inhomogeneous model					
200	50	0.860	0.769	0.659	0.510
400	100	0.997	0.991	0.967	0.873
800	200	1	1	1	0.999

Table 27 Proportion of rejections for different alternative hypotheses (deviation from the null hypothesis controlled by parameter a) for the KS type test statistic on *Dendrite*

Homogeneous model					
m_1	m_2	a=$7m_2/4$	$a = 3m_2/2$	$a = 5m_2/4$	$a = m_2$
50	200	0.187	0.189	0.195	0.189
100	400	0.454	0.459	0.440	0.400
200	800	0.911	0.885	0.846	0.800
500	2000	1	1	1	1
Inhomogeneous model					
50	200	0.204	0.215	0.217	0.209
100	400	0.473	0.473	0.451	0.392
200	800	0.895	0.864	0.850	0.784
500	2000	1	1	1	1

Table 28 Proportion of rejections under the null hypothesis for the Cramér von Mises type test statistic on the subnetwork of *Spiders*

		Homogeneous model			Inhomogeneous model		
m_1	m_2	$\alpha = 0.1$	$\alpha = 0.05$	$\alpha = 0.01$	$\alpha = 0.1$	$\alpha = 0.05$	$\alpha = 0.01$
20	80	0.099	0.048	0.012	0.103	0.055	0.012
50	200	0.089	0.048	0.010	0.097	0.050	0.011
100	400	0.083	0.031	0.009	0.106	0.053	0.009
200	800	0.100	0.045	0.005	0.119	0.060	0.007
500	2000	0.107	0.054	0.012	0.089	0.045	0.012
750	3000	0.104	0.053	0.011	0.086	0.039	0.005

Table 29 Proportion of rejections under the null hypothesis for the Cramér von Mises type test statistic on the subnetwork of *Dendrite*

		Homogeneous model			Inhomogeneous model		
m_1	m_2	$\alpha = 0.1$	$\alpha = 0.05$	$\alpha = 0.01$	$\alpha = 0.1$	$\alpha = 0.05$	$\alpha = 0.01$
20	80	0.099	0.054	0.009	0.109	0.055	0.010
50	200	0.095	0.051	0.011	0.085	0.042	0.009
100	400	0.090	0.048	0.008	0.106	0.051	0.008
200	800	0.100	0.044	0.008	0.095	0.043	0.008
500	2000	0.108	0.050	0.010	0.103	0.048	0.012
750	3000	0.116	0.061	0.008	0.115	0.058	0.010

Table 30 Proportion of rejections for different alternative hypotheses (deviation from the null hypothesis controlled by parameter a) for the Cramér von Mises type test statistic on the subnetwork of *Spiders*

		Homogeneous model			Inhomogeneous model		
m_1	m_2	$a = 3m_2/4$	$a = m_2/2$	$a = m_2/4$	$a = 3m_2/4$	$a = m_2/2$	$a = m_2/4$
200	50	0.998	0.909	0.383	0.991	0.858	0.370
400	100	1	0.998	0.699	1	0.998	0.657
800	200	1	1	0.951	1	1	0.949
2000	500	1	1	1	1	1	1

Table 31 Proportion of rejections for different alternative hypotheses (deviation from the null hypothesis controlled by parameter a) for the Cramér von Mises type test statistic on the subnetwork of *Dendrite*

		Homogeneous model			Inhomogeneous model		
m_1	m_2	$a = 3m_2/4$	$a = m_2/2$	$a = m_2/4$	$a = 3m_2/4$	$a = m_2/2$	$a = m_2/4$
200	50	1	0.974	0.546	1	0.980	0.575
400	100	1	0.999	0.867	1	1	0.872
800	200	1	1	0.995	1	1	0.999
2000	500	1	1	1	1	1	1

Table 32 Proportion of rejections for different alternative hypotheses (deviation from the null hypothesis controlled by parameter a) for the Cramér von Mises type test statistic on the subnetwork of *Spiders*

		Homogeneous model			Inhomogeneous model		
m_1	m_2	$a = 3m_2/4$	$a = m_2/2$	$a = m_2/4$	$a = 3m_2/4$	$a = m_2/2$	$a = m_2/4$
50	200	0.986	0.846	0.294	0.988	0.865	0.319
100	400	1	0.997	0.663	1	0.999	0.656
200	800	1	1	0.970	1	1	0.952
500	2000	1	1	1	1	1	1

Table 33 Proportion of rejections for different alternative hypotheses (deviation from the null hypothesis controlled by parameter a) for the Cramèr von Mises type test statistic on the subnetwork of *Dendrite*

		Homogeneous model			Inhomogeneous model		
m_1	m_2	$a = 3m_2/4$	$a = m_2/2$	$a = m_2/4$	$a = 3m_2/4$	$a = m_2/2$	$a = m_2/4$
50	200	0.998	0.972	0.582	1	0.973	0.597
100	400	1	1	0.875	1	1	0.893
200	800	1	1	0.996	1	1	0.998
500	2000	1	1	1	1	1	1

Supplementary Information The online version contains supplementary material available at https://doi.org/10.1007/s00362-024-01657-8.

Acknowledgements The authors are grateful for the very constructive comments from the two anonymous reviewers which helped to improve this manuscript. María Isabel Borrajo and Wenceslao González-Manteiga acknowledge the support of from Grant PID2020-116587GB-I00 funded by MCIN/AEI/10.13039/501100011033 and the European Union. Ignacio González-Pérez thanks the Barrié Foundation, of which he is a Fellow of the 2022 call, for their support throughout his graduate studies. The authors also acknowledge the contribution of professor Rodrigo Targino, Assistant Professor in Statistics at the School of Applied Mathematics at Getulio Vargas Foundation, for his contribution by providing the data set about traffic accidents in Rio de Janeiro analysed here.

Funding Open Access funding provided thanks to the CRUE-CSIC agreement with Springer Nature. Funding was provided by MCIN/AEI/10.13039/501100011033 (PID2020-116587GB-I00).

Declarations

Conflict of interest The authors have no relevant financial or non-financial interests to disclose.

References

Alba-Fernández V, Jiménez-Gamero MD, Muñoz-Garcia J (2008) A test for the two-sample problem based on empirical characteristic functions. Comput Stat Data Anal 52(7):3730–3748. https://doi.org/10.1016/j.csda.2007.12.013

Anderes E, Møller J, Rasmussen JG (2020) Isotropic covariance functions on graphs and their edges. Ann Stat 48(4):2478–2503. https://doi.org/10.1214/19-AOS1896

Anderson NH, Hall P, Titterington DM (1994) Two-sample test statistics for measuring discrepancies between two multivariate probability density functions using kernel-based density estimates. J Multivar Anal 50(1):41–54. https://doi.org/10.1006/jmva.1994.1033

Ang QW, Baddeley A, Nair G (2012) Geometrically corrected second order analysis of events on a linear network, with applications to ecology and criminology. Scand J Stat 39(4):591–617. https://doi.org/10.1111/j.1467-9469.2011.00752.x

Bacchieri G, Barros AJD (2011) Traffic accidents in brazil from 1998 to 2010: many changes and few effects. Rev Saude Publica 45:949–963. https://doi.org/10.1590/S0034-89102011005000069

Baddeley A, Turner R (2005) Spatstat: an r package for analyzing spatial point patterns. J Stat Softw 12:1–42. https://doi.org/10.18637/jss.v012.i06

Baddeley A, Jammalamadaka A, Nair G (2014) Multitype point process analysis of spines on the dendrite network of a neuron. J R Stat Soc 63(5):673–694. https://doi.org/10.1111/rssc.12054

Baddeley A, Rubak E, Turner R (2015) Spatial point patterns: methodology and applications with R. CRC Press, Boca Raton

Baddeley A, Nair G, Rakshit S, McSwiggan G, Davies TM (2021) Analysing point patterns on networks—a review. Spatial Stat 42:100435. https://doi.org/10.1016/j.spasta.2020.100435

Bertanha M, Chung E (2023) Permutation tests at nonparametric rates. J Am Stat Assoc 118(544):2833–2846. https://doi.org/10.1080/01621459.2022.2087660

Borrajo MI, González-Manteiga W, Martínez-Miranda MD (2020) Testing for significant differences between two spatial patterns using covariates. Spatial Stat 40:100379. https://doi.org/10.1016/j.spasta.2019.100379

Borruso G (2005) Network density estimation: analysis of point patterns over a network. In: International conference on computational science and its applications, pp 126–132

Borruso G (2008) Network density estimation: a GIS approach for analysing point patterns in a network space. Trans GIS 12(3):377–402. https://doi.org/10.1111/j.1467-9671.2008.01107.x

Briz-Redón Á, Martínez-Ruiz F, Montes F (2019) Estimating the occurrence of traffic accidents near school locations: a case study from Valencia (Spain) including several approaches. Accid Anal Prev 132:105237. https://doi.org/10.1016/j.aap.2019.07.013

Chu L, Dai X (2024) Manifold energy two-sample test. Electron J Stat 18(1):145–166. https://doi.org/10.1214/23-EJS2203

Corral-Rivas JJ, Wehenkel C, Castellanos-Bocaz HA, Vargas-Larreta B, Diéguez-Aranda U (2010) A permutation test of spatial randomness: application to nearest neighbour indices in forest stands. J For Res 15(4):218–225. https://doi.org/10.1007/s10310-010-0181-1

Cressie N (2015) Statistics for spatial data. Wiley, New York

Cronie O, Moradi M, Mateu J (2020) Inhomogeneous higher-order summary statistics for point processes on linear networks. Stat Comput 30(5):1221–1239. https://doi.org/10.1007/s13253-024-00605-1

Cronie O, Jansson J, Konstantinou K (2024) Discussion of the paper "marked spatial point processes: Current state and extensions to point processes on linear networks". J Agric Biol Environ Stat 29(2):379–388. https://doi.org/10.1007/s13253-024-00606-0

Daley DJ, Vere-Jones D et al (2003) An introduction to the theory of point processes: volume I: elementary theory and methods. Springer, London

D'Angelo N, Adelfio G, Abbruzzo A, Mateu J (2022) Inhomogeneous spatio-temporal point processes on linear networks for visitors' stops data. Ann Appl Stat 16(2):791–815. https://doi.org/10.1214/21-AOAS1519

D'Angelo N, Adelfio G, Mateu J (2023) Local inhomogeneous second-order characteristics for spatio-temporal point processes occurring on linear networks. Stat Pap 64(3):779–805. https://doi.org/10.1007/s00362-022-01338-4

Dantzig GB, Thapa MN (1997) Linear programming: introduction, vol 1. Springer, Berlin

Dantzig GB, Thapa MN (2003) Linear programming: theory and extensions, vol 2. Springer, Berlin

Davies TM, Marshall JC, Hazelton ML (2018) Tutorial on kernel estimation of continuous spatial and spatiotemporal relative risk. Stat Med 37(7):1191–1221. https://doi.org/10.1002/sim.7577

Diggle PJ (2013) Statistical analysis of spatial and spatio-temporal point patterns. CRC Press, Boca Raton

Eckardt M, Mateu J (2018) Point patterns occurring on complex structures in space and space-time: an alternative network approach. J Comput Graph Stat 27(2):312–322. https://doi.org/10.1080/10618600.2017.1391695

Eckardt M, Mateu J (2021) Second-order and local characteristics of network intensity functions. TEST 30(2):318–340. https://doi.org/10.1007/s11749-020-00720-4

Eckardt M, Moradi M (2024) Marked spatial point processes: current state and extensions to point processes on linear networks. J Agric Biol Environ Stat 29:346–378. https://doi.org/10.1007/s13253-024-00605-1

Finner H, Gontscharuk V (2018) Two-sample kolmogorov-smirnov-type tests revisited: old and new tests in terms of local levels. Ann Stat 46(6A):3014–3037

Foxall R, Baddeley A (2002) Nonparametric measures of association between a spatial point process and a random set, with geological applications. J R Stat Soc 51(2):165–182. https://doi.org/10.1111/1467-9876.00261

Fuentes-Santos I, González-Manteiga W, Mateu J (2016) Consistent smooth bootstrap kernel intensity estimation for inhomogeneous spatial Poisson point processes. Scand J Stat 43(2):416–435. https://doi.org/10.1111/sjos.12183

Fuentes-Santos I, González-Manteiga W, Mateu J (2018) A first-order, ratio-based nonparametric separability test for spatiotemporal point processes. Environmetrics. https://doi.org/10.1002/env.2482

Fuentes-Santos I, González-Manteiga W, Mateu J (2023) Testing similarity between first-order intensities of spatial point processes. A comparative study. Commun Stat Simul Comput 52(5):2210–2230. https://doi.org/10.1080/03610918.2021.1901118

Ghadirzadeh M, Shojaei A, Khademi A, Khodadoost M, Kandi M, Alaeddini F, Moradi S (2015) Status and trend of deaths due to traffic accidents from 2001 to 2010 in Iran. Iran J Epidemiol 11(2):13–22

González-Manteiga W, Crujeiras RM (2013) An updated review of goodness-of-fit tests for regression models. TEST 22:361–411. https://doi.org/10.1007/s11749-013-0327-5

Google (2022) Google maps. https://www.google.es/maps/@-22.9140693,-43.5860658,11z?hl=es. Accessed 5 June 2022

Gopalakrishnan S (2012) A public health perspective of road traffic accidents. J Fam Med Primary Care 1(2):144. https://doi.org/10.4103/2249-4863.104987

Gu J, Tan R, Yin G (2024) Delaunay weighted two-sample test for high-dimensional data by incorporating geometric information. arXiv:2404.03198

Horowitz JL, Spokoiny VG (2001) An adaptive, rate-optimal test of a parametric mean-regression model against a nonparametric alternative. Econometrica 69(3):599–631. https://doi.org/10.1111/1468-0262.00207

Illian JB, Møller J, Waagepetersen RP (2009) Hierarchical spatial point process analysis for a plant community with high biodiversity. Environ Ecol Stat 16:389–405. https://doi.org/10.1007/s10651-007-0070-8

Jammalamadaka A, Banerjee S, Manjunath BS, Kosik KS (2013) Statistical analysis of dendritic spine distributions in rat hippocampal cultures. BMC Bioinf 14:1–19. https://doi.org/10.1186/1471-2105-14-287

Khismatullina M, Vogt M (2023) Nonparametric comparison of epidemic time trends: the case of COVID-19. J Econom 232(1):87–108. https://doi.org/10.1016/j.jeconom.2021.04.010

Law R, Illian J, Burslem DFRP, Gratzer G, Gunatilleke CVS, Gunatilleke I (2009) Ecological information from spatial patterns of plants: insights from point process theory. J Ecol 97(4):616–628. https://doi.org/10.1111/j.1365-2745.2009.01510.x

Lawson AB (2013) Statistical methods in spatial epidemiology. Wiley, New York

Loosmore NB, Ford ED (2006) Statistical inference using the G or K point pattern spatial statistics. Ecology 87(8):1925–1931. https://doi.org/10.1890/0012-9658(2006)87[1925:SIUTGO]2.0.CO;2

Marozzi M (2004) Some remarks about the number of permutations one should consider to perform a permutation test. Statistica (Bologna) 64(1):193–201. https://doi.org/10.6092/issn.1973-2201/32

McSwiggan G (2019) Spatial point process methods for linear networks with applications to road accident analysis. Doctoral dissertation, The University of Western Australia. https://doi.org/10.26182/5f057c45c007e

McSwiggan G, Baddeley A, Nair G (2017) Kernel density estimation on a linear network. Scand J Stat 44(2):324–345. https://doi.org/10.1111/sjos.12255

Møller J, Rasmussen JG (2024) Cox processes driven by transformed gaussian processes on linear networks. Scand J Stat. https://doi.org/10.1111/sjos.12720

Moradi MM (2018) Spatial and spatio-temporal point patterns on linear networks. Doctoral dissertation, Universidade NOVA de Lisboa (Portugal). https://doi.org/10.6035/14123.2018.685382

Moradi MM, Mateu J (2020) First-and second-order characteristics of spatio-temporal point processes on linear networks. J Comput Graph Stat 29(3):432–443. https://doi.org/10.1080/10618600.2019.1694524

Moradi MM, Rodríguez-Cortés FJ, Mateu J (2018) On kernel-based intensity estimation of spatial point patterns on linear networks. J Comput Graph Stat 27(2):302–311. https://doi.org/10.1080/10618600.2017.1360782

Moradi MM, Cronie O, Rubak E, Lachieze-Rey R, Mateu J, Baddeley A (2019) Resampling smoothing of Voronoi intensity estimators. Stat Comput 29(5):995–1010. https://doi.org/10.1007/s11222-018-09850-0

Myllymaki M, Mrkvicka T, Grabarnik P, Seijo H, Hahn U (2017) Global envelope tests for spatial point patterns. J R Stat Soc Ser B (Stat Methodol) 79:381–404. https://doi.org/10.1111/insr.12327

Ogata Y, Zhuang J (2006) Space-time etas models and an improved extension. Tectonophysics 413(1–2):13–23. https://doi.org/10.1016/j.tecto.2005.10.016

Okabe A, Sugihara K (2012) Spatial analysis along networks: statistical and computational methods. Wiley, New York

Okabe A, Yamada I (2001) The K-function method on a network and its computational implementation. Geogr Anal 33(3):271–290. https://doi.org/10.1111/j.1538-4632.2001.tb00448.x

Okabe A, Satoh T, Sugihara K (2009) A kernel density estimation method for networks, its computational method and a GIS-based tool. Int J Geogr Inf Sci 23(1):7–32. https://doi.org/10.1080/13658810802475491

Pesarin F, Salmaso L (2010) Finite-sample consistency of combination-based permutation tests with application to repeated measures designs. J Nonparametr Stat 22(5):669–684. https://doi.org/10.1080/10485250902807407

Pesarin F, Salmaso L (2013) On the weak consistency of permutation tests. Commun Stat Simul Comput 42(6):1368–1379. https://doi.org/10.1080/03610918.2012.625338

Rakshit S, Davies T, Moradi MM, McSwiggan G, Nair G, Mateu J, Baddeley A (2019) Fast kernel smoothing of point patterns on a large network using two-dimensional convolution. Int Stat Rev 87(3):531–556. https://doi.org/10.1111/insr.12327

Ripley BD (1977) Modelling spatial patterns. J R Stat Soc Ser B (Methodol) 39(2):172–192. https://doi.org/10.1111/j.2517-6161.1977.tb01615.x

Ripley BD (2005) Spatial statistics. Wiley, New York

Schoenberg FP (2003) Multidimensional residual analysis of point process models for earthquake occurrences. J Am Stat Assoc 98(464):789–795. https://doi.org/10.1198/016214503000000710

Stoyan D, Penttinen A (2000) Recent applications of point process methods in forestry statistics. Stat Sci 15(1):61–78

van Lieshout M (2018) Nearest-neighbour Markov point processes on graphs with Euclidean edges. Adv Appl Probab 50(4):1275–1293. https://doi.org/10.1017/apr.2018.60

Voss S (1999) Habitat preferences and spatial dynamics of the urban wall spider: *Oecobius annulipes* Lucas (Unpublished doctoral dissertation). University of Western Australia

Voss SC, Main BY, Dadour IR (2007) Habitat preferences of the urban wall spider *Oecobius navus* (Araneae, Oecobiidae). Aust J Entomol 46(4):261–268. https://doi.org/10.1111/j.1440-6055.2007.00616.x

WHO (2023) Road traffic mortality. https://www.who.int/data/gho/data/themes/topics/topic-details/GHO/road-traffic-mortality. Accessed 29 Nov 2023

Xie Z, Yan J (2008) Kernel density estimation of traffic accidents in a network space. Comput Environ Urban Syst 32(5):396–406. https://doi.org/10.1016/j.compenvurbsys.2008.05.001

Yang BM, Kim J (2003) Road traffic accidents and policy interventions in Korea. Int Control Saf Promot 10(1–2):89–94. https://doi.org/10.1076/icsp.10.1.89.14120

Zhang T, Zhuang R (2017) Testing proportionality between the first-order intensity functions of spatial point processes. J Multivar Anal 155:72–82. https://doi.org/10.1016/j.jmva.2016.11.013

Zheng Z, Wang Z, Liu S, Ma W (2024) Exploring the spatial effects on the level of congestion caused by traffic accidents in urban road networks: a case study of beijing. Travel Behav Soc 35:100728. https://doi.org/10.1016/j.tbs.2023.100728